MULTISCALE MODEL. SIMUL.
Vol. 8, No. 5, pp. 1981–2022

SOURCE LOCALIZATION IN RANDOM ACOUSTIC WAVEGUIDES*

LILIANA BORCEA†, LEILA ISSA†, AND CHRYSOULA TSOGKA‡

Abstract. Mode coupling due to scattering by weak random inhomogeneities in waveguides leads to loss of coherence of wave fields at long distances of propagation. This in turn leads to serious deterioration of coherent source localization methods, such as matched field. We study with analysis and numerical simulations how such deterioration occurs and introduce a novel incoherent approach for long range source localization in random waveguides. It is based on a special form of transport theory for the incoherent fluctuations of the wave field. We study theoretically the statistical stability of the method and illustrate its performance with numerical simulations. We also show how it can be used to estimate the correlation function of the random fluctuations of the wave speed.

Key words. array imaging, randomly layered media, local cosine transform

AMS subject classifications. 35R60, 35R30, 60G35

DOI. 10.1137/100782711

1. Introduction.

The problem of source localization with a remote array of sensors in a waveguide has been the topic of many studies in underwater acoustics. The localization is often done with matched field and related coherent methods [1, 18], which match the acoustic pressure $p(t, \vec{x})$ received at the array with its mathematical model, for hypothetical source locations in a search domain. Matched field methods deal well with additive noise, but they are sensitive to inaccuracies in the model of $p(t, \vec{x})$, due, for example, to unknown perturbations in the waveguide geometry and the sound speed. Although such perturbations are typically small [10], they can have a significant cumulative effect on sound transmission at long ranges [10, 9, 14].

In this paper we study theoretically and numerically source localization in waveguides with random inhomogeneities. In the absence of such inhomogeneities, energy propagates through guided wave modes that do not interact with each other. Scattering by the random inhomogeneities induces mode coupling. When the coupling effects are weak, they can be approximated via a first order perturbation analysis of the eigenvalue problem for the modes [15]. Alternatively, the matched field algorithms can be improved with some statistical signal processing that mitigates the effect of the inhomogeneities on the array data [19, 13].

We study source localization at very long ranges, where the cumulative effect of the random inhomogeneities is strong, and there is little coherence in the field $p(t, \vec{x})$ received at the array. We show through analysis and numerical simulations

*Received by the editors January 14, 2010; accepted for publication (in revised form) September 9, 2010; published electronically December 7, 2010.

http://www.siam.org/journals/mms/8-5/78271.html

†Department of Computational and Applied Mathematics, Rice University, MS 134, Houston, TX 77005-1892 (borcea@caam.rice.edu, issa@caam.rice.edu). The work of the first author was partially supported by National Science Foundation grants DMS-0604008, DMS-0934594, and DMS-0907746 and Office of Naval Research grants N000140910290 and N000140510699. The work of the second author was partially supported by Office of Naval Research grant N000140510699 and National Science Foundation grant DMS-0604008.

‡Department of Applied Mathematics, University of Crete, GR-71409 Heraklion, Greece, and IACM/FORTH, GR-71110 Heraklion, Greece (tsogka@tem.uoc.gr). The work of this author was partially supported by European Research Council starting grant GA 239959 and European FP7 Marie Curie International reintegration grant MIRG-CT-2007-203438.

how coherent imaging methods fail to give useful results in such scattering regimes and introduce a novel incoherent source localization approach. The analysis is based on the asymptotic theory of wave propagation in random waveguides developed in [14, 9, 12, 11]. The asymptotics is in the amplitude scale $\varepsilon \ll 1$ of the random fluctuations of the wave speed and for very long distances of propagation.

In general, the waveguide effect can be due to confining boundaries or to the transverse sound speed profile. We consider waveguides with confining horizontal planar boundaries, and assume for simplicity random fluctuations of the sound speed in range and depth (cross-range), so that we can reduce the problem to two dimensions. The general three dimensional problem does not introduce essential difficulties in the analysis [14], but it is prohibitively expensive for the numerical simulations.

The wave propagation study in [14] is more comprehensive, because it incorporates radiation in the ocean floor modeled as a half-space. It is complicated by the fact that aside from the discrete (trapped) modes, there is the continuum (radiation) spectrum. However, it turns out that, asymptotically, the statistical properties of the trapped mode amplitudes can be described independently of the amplitudes of the radiation modes [14, section 3]. Since the behavior of source localization methods depends on the statistics of propagating trapped modes, we expect that our analysis and results extend to the more general setup in [14].

The paper is organized as follows. We begin in section 2 with the formulation of the source localization problem in waveguides, and we describe three coherent source localization methods: synthetic back propagation of the time reversed array data in an unperturbed (deterministic) waveguide; matched field; and coherent interferometry. The numerical simulations in section 3 illustrate how these methods fail to localize sources at long ranges in random waveguides. The remainder of the paper is concerned with a theoretical explanation of the results in section 3 and with the formulation and analysis of a novel incoherent source localization approach. The mathematical model of the array data is in section 4. We use this model in section 5 to obtain a detailed theoretical explanation of the failure of coherent source localization methods. Section 6 introduces our incoherent source localization approach, based on a special form of transport theory developed in [12, 11] for the incoherent wave fluctuations. We study the statistical stability of our method with respect to the realizations of the random medium and illustrate its performance with numerical simulations. We also show how it can be used to estimate the correlation function of the random fluctuations of the sound speed. We end in section 7 with a summary.

2. Formulation of the source localization problem. We consider a two dimensional waveguide with range axis denoted by $z \in \mathbb{R}$ and transverse (cross-range) coordinate $x \in (0, X)$. The acoustic pressure field $p(t, \vec{x})$ satisfies the wave equation

$$\Delta p(t,\vec{x}) - \frac{1}{c^2(\vec{x})}\frac{\partial^2 p(t,\vec{x})}{\partial t^2} = \nabla \cdot \vec{F}(t,\vec{x}) \tag{2.1}$$

for time $t > 0$ and $\vec{x} = (x, z)$. Here $c(\vec{x})$ is the sound speed and

$$\vec{F}(t,\vec{x}) = f(t)\delta(\vec{x} - \vec{x}_\star)\vec{e}_z \tag{2.2}$$

models a point-like source at $\vec{x}_\star$, emitting a pulse $f(t)$ in the range direction $\vec{e}_z$, toward the array. Before the pulse emission, the medium is quiescent:

$$p(t,\vec{x}) \equiv 0, \qquad t \le 0. \tag{2.3}$$

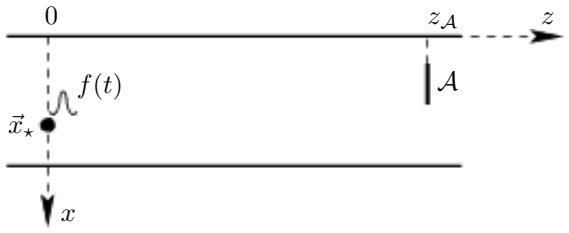

FIG. 2.1. *Schematic of the source localization problem setup.*

We assume as in [12, 11] pressure release boundary conditions at the top and bottom of the waveguide:

$$p(t,\vec{x}) = 0, \qquad x \in \{0, X\}. \tag{2.4}$$

We could consider other conditions, such as $\partial p/\partial x = 0$ at $x = X$, corresponding to a rigid bottom, but there is no essential difference in the analysis.

Let us take the Fourier transform

$$\widehat{p}(\omega,\vec{x}) = \int e^{i\omega t} p(t,\vec{x})\, dt \tag{2.5}$$

and obtain from (2.1) the Helmholtz equation

$$\Delta\widehat{p}(\omega,\vec{x}) + \frac{\omega^2}{c^2(\vec{x})}\widehat{p}(\omega,\vec{x}) = \widehat{f}(\omega)\frac{\partial}{\partial z}\delta(\vec{x}-\vec{x}_\star), \tag{2.6}$$

with derivatives in the sense of distributions. In ideal waveguides, the sound speed varies only in the transverse direction and energy is transmitted by independent guided modes, the orthogonal eigenfunctions of the symmetric differential operator $\partial_x^2 + \omega^2/c^2(x)$. We consider waveguides with random inhomogeneities, caused, for example, by internal waves, where $c(\vec{x})$ has an (x,z)-dependent fluctuating part, with weak amplitudes of the order 1%–3%, as is typical in underwater acoustics [10, 9, 14]. Wave scattering in such waveguides leads to mode coupling and loss of coherence of the acoustic pressure field and impedes source localization at long ranges.

The schematic for the source localization problem is in Figure 2.1. We have an array $\mathcal{A}$ at very long distance $z_{\mathcal{A}}$ from the source, with receivers at transverse coordinates r. The receivers record the acoustic pressure field $p(t, r, z_{\mathcal{A}})$ over some time window, and the problem is to estimate the location $\vec{x}_\star$ of the source from the array data.

Note that we consistently use a coordinate system with range origin at the source, so that $\vec{x}_\star = (x_\star, 0)$. The unknowns in the source localization problem are therefore $x_\star$ and $z_{\mathcal{A}}$.

2.1. Coherent source localization. We define here three coherent source localization functions. Then, we illustrate in section 3 how they fail to give useful results because of strong cumulative scattering in random waveguides at long ranges. The detailed theoretical explanation is in section 5.

The first coherent source localization function is given by

$$\mathcal{I}(\vec{x}^s) = \int \frac{d\omega}{2\pi} \sum_{r\in\mathcal{A}} \overline{\widehat{p}}(\omega, r, z_{\mathcal{A}})\widehat{G}_o(\omega, r, z_{\mathcal{A}}; \vec{x}^s), \tag{2.7}$$

where the bar denotes complex conjugation, and $\widehat{G}_o(\omega, x, z; \vec{x}^s)$ is the Green's function of Helmholtz's equation in the unperturbed waveguide. Expression (2.7) models the time reversal of the pressure field $p(t, r, z_{\mathcal{A}})$ recorded at the receivers, and its re-emission in the fictitious unperturbed waveguide, where we "observe" the wave field at the search point $\vec{x}^s$, the hypothetical source location. If the array records up to time T, the Fourier coefficients of the time reversed $p(T-t, r, z_{\mathcal{A}})$ are $\overline{\widehat{p}}(\omega, r, z_{\mathcal{A}})e^{i\omega T}$. Functional (2.7) amounts to observing the time reversed field at time lag T after its re-emission, when it is expected to refocus.

In the absence of the random fluctuations, $\mathcal{I}(\vec{x}^s) = \mathcal{I}_o^{TR}(\vec{x}^s)$, the time reversal function, which focuses at $\vec{x}^s = \vec{x}_\star$. In random waveguides, $\mathcal{I}(\vec{x}^s)$ does not model the time reversal process, because the back propagation is synthetic, via the unperturbed Green's function $\widehat{G}_o$. Time reversal is an experiment where the back propagation is done in the actual random waveguide, and focusing can be observed around $\vec{x}_\star$ with improved resolution and in a statistically stable manner, as proved in [12] and demonstrated experimentally in [16]. Time reversal cannot be used for source localization, and back propagation in the fictitious unperturbed waveguide does not work well, as we show in the next section.

Coherent interferometry (CINT) was introduced in [4, 5] for imaging in random, open environments. It back propagates to $\vec{x}^s$ cross-correlations of the traces of the acoustic pressure at the array, instead of the traces themselves as in $\mathcal{I}(\vec{x}^s)$. The cross-correlations are over suitable time and receiver offset windows, and they introduce a statistical smoothing in the imaging process for achieving stability [6]. The optimal smoothing is determined by two decoherence parameters intrinsic to the data: the decoherence length X_d and frequency Ω_d [5, 6]. The decoherence length is the receiver offset $|r - r'|$ over which $\widehat{p}(\omega, r, z_{\mathcal{A}})$ and $\widehat{p}(\omega, r', z_{\mathcal{A}})$ become statistically uncorrelated. Similarly, Ω_d is the frequency lag $|\omega - \omega'|$ over which $\widehat{p}(\omega, r, z_{\mathcal{A}})$ and $\widehat{p}(\omega', r, z_{\mathcal{A}})$ become uncorrelated. It follows from [14, 9, 11] (see also Lemmas 5.1 and 5.2) that in random waveguides, at long source-array ranges, there is no decorrelation over the receiver offset,

$$E\left\{\widehat{p}(\omega, r, z_{\mathcal{A}})\overline{\widehat{p}}(\omega, r', z_{\mathcal{A}})\right\} \not\approx E\left\{\widehat{p}(\omega, r, z_{\mathcal{A}})\right\} E\left\{\overline{\widehat{p}}(\omega, r', z_{\mathcal{A}})\right\} \quad \text{for all} \quad r, r' \in (0, X),$$

but there is rapid decorrelation over the frequency (Ω_d is small). Thus, CINT reduces to back propagating the cross-correlation of the received traces across the array over long time windows $\chi_{\Omega_d}(t)$ of support Ω_d^{-1}:

$$\begin{aligned}\mathcal{I}^{CINT}(\vec{x}^s) = \int \frac{d\omega}{2\pi} \int \frac{d\omega'}{2\pi} \widehat{\chi}_{\Omega_d}(\omega - \omega') \sum_{r \in \mathcal{A}} \widehat{p}(\omega, r, z_{\mathcal{A}}) \overline{\widehat{G}_o}(\omega, r, z_{\mathcal{A}}; \vec{x}^s) \\ \times \sum_{r' \in \mathcal{A}} \overline{\widehat{p}}(\omega', r', z_{\mathcal{A}}) \widehat{G}_o(\omega', r', z_{\mathcal{A}}; \vec{x}^s). \end{aligned} \tag{2.8}$$

When we replace $\widehat{\chi}_{\Omega_d}/(2\pi)$ with the Dirac δ distribution, we ignore frequency correlations and get the conventional (Bartlett) matched field function

$$\mathcal{I}^{MF}(\vec{x}^s) = \int \frac{d\omega}{2\pi} \left| \sum_{r \in \mathcal{A}} \overline{\widehat{p}}(\omega, r, z_{\mathcal{A}}) \widehat{G}_o(\omega, r, z_{\mathcal{A}}; \vec{x}^s) \right|^2 . \tag{2.9}$$

There are better matched field methods for source localization that include some signal processing to mitigate additive noise or mild clutter effects [1, 15]. Nevertheless, all these methods rely on a coherent $p(t, r, z_{\mathcal{A}})$, and their behavior should be similar

to (2.9) at long ranges from the source, where cumulative scattering by the random inhomogeneities is strong.

3. Numerical simulations. We use numerical simulations to illustrate the performance of source localization methods in random waveguides. We simulate the array data $p(t, r, z_{\mathcal{A}})$ by solving the wave equation as a first order velocity-pressure system with the finite element method given in [2] in two dimensions. The setup is illustrated in Figure 3.1, with the source at $(x_\star, 0)$ and the array $\mathcal{A}$ at range $z_{\mathcal{A}}$. We use two perfectly matched layers (PMLs) to the left and right of the computational domain to model the unbounded waveguide in z.

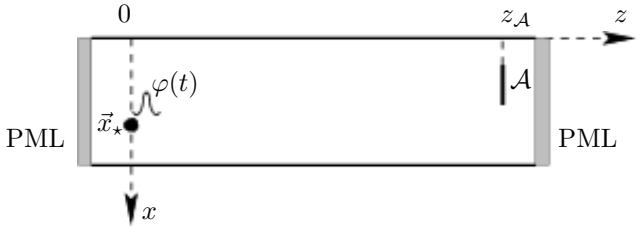

FIG. 3.1. *Setup for the numerical simulations.*

We take fluctuations of the sound speed of the form

$$\frac{c_o^2}{c^2(\vec{x})} = 1 + \varepsilon\nu(\vec{x}), \tag{3.1}$$

with $\nu(\vec{x})$ an isotropic, statistically homogeneous random process with mean zero and Gaussian correlation

$$E\{\nu(\vec{x})\nu(\vec{x}')\} = \frac{1}{2\pi\ell^2} e^{-\frac{|\vec{x}-\vec{x}'|^2}{2\ell^2}}. \tag{3.2}$$

We generate the process numerically using random Fourier series [8]. The correlation length is $\ell = 0.25$m, and the perturbation parameter ε ranges between 1%–3%. We choose a constant background speed c_o to simplify the back propagation in the unperturbed waveguide by computing $\widehat{G}_o(\omega, r, z_{\mathcal{A}}; \vec{x}^s)$ explicitly.

The range $z_{\mathcal{A}}$ is long, of order ε^{-2}, and the Fourier coefficients $\widehat{p}(\omega, r, z_{\mathcal{A}})$ of the array data decorrelate rapidly in frequency ($\Omega_d = \varepsilon^2\Omega$) as shown in [14, 9, 11]. To explore the effect of the bandwidth and central frequency on source localization, we let the source excitation be a short pulse $\varphi(t)$ (a sinc function, with Fourier transform given by the indicator function of the frequency bandwidth), with bandwidth 1.5–4.5kHz measured at 6dB. Then, we define $f(t)$ as the signal with Fourier transform

$$\widehat{f}(\omega) = \widehat{f}^{\varepsilon}(\omega) = \widehat{\varphi}(\omega) 1_{[-B,B]}\left(\frac{\omega - \omega_o}{\varepsilon^\sigma}\right), \tag{3.3}$$

where $1_{[-B,B]}$ is the characteristic function of interval $[-B, B]$. That is, $\widehat{f}^{\varepsilon}(\omega)$ is the windowed $\widehat{\varphi}(\omega)$ in the frequency interval $|\omega - \omega_o| \le \varepsilon^\sigma B$ for various choices of ω_o in the band of $\widehat{\varphi}$, and $\sigma \in [0, 2]$. The scaled bandwidth B is some $O(1)$ factor of ω_o. We refer to the case $\sigma = 2$ as narrow band, because the bandwidth $\varepsilon^2 B$ is of the same order as the decoherence frequency, and the support of the pulse $f^{\varepsilon}(t)$ is a time interval of length similar to that of the travel time. Broad band signals with $\sigma < 2$

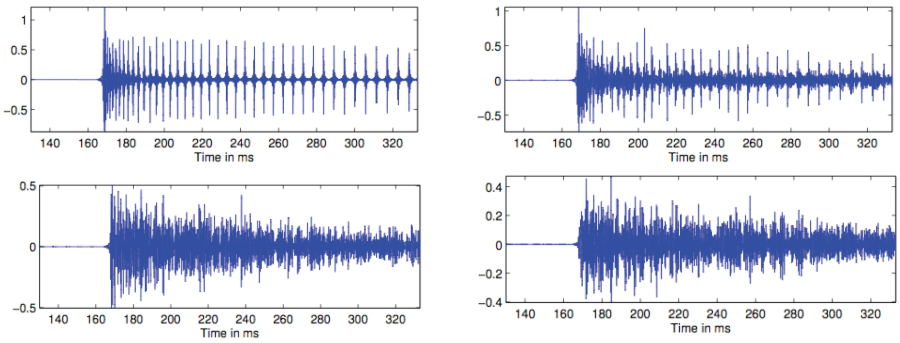

FIG. 3.2. *The trace of the acoustic pressure computed at the receiver location* $(r = X/2, z_{\mathcal{A}})$ *for (clockwise from top left)* $\varepsilon = 0$, $\varepsilon = 1\%$, $\varepsilon = 2\%$, *and* $\varepsilon = 3\%$.

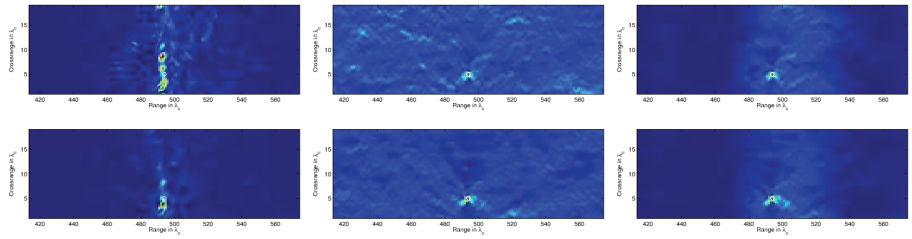

FIG. 3.3. *From left to right:* $\mathcal{I}(\vec{x}^s)$, $\mathcal{I}^{MF}(\vec{x}^s)$, *and* $\mathcal{I}^{CINT}(\vec{x}^s)$ *for the source at* $x_\star = X/4$. *Row one is for one realization of the medium and row two for another. The results are for* $\varepsilon = 2\%$, *central frequency* $2.09kHz$, *and bandwidth* $0.375kHz$. *The CINT images are computed with* $\Omega_d = 0.045kHz$. *The abscissa of the images is range scaled by* λ_c, *and the ordinate is cross-range scaled by* λ_c.

have a time support that is much smaller than the travel time, and we can observe at the array the arrival of different waveguide modes.

All the lengths are scaled by the central wavelength $\lambda_c = 0.5$m of the pulse $\varphi(t)$, computed with $c_o = 1.5$km/s. The computational domain is the rectangle of transverse side length $X = 20\lambda_c$ and range length $500\lambda_c$. The source is $4\lambda_c$ away from the left PML at either $x_\star = X/2$ or $x_\star = X/4$. The array is at range $z_{\mathcal{A}} = 494\lambda_c$ from the source, and its aperture $\mathcal{A}$ consists of various intervals in $[0, X]$.

The numerically simulated array data is the computed pressure $p(t, r, z_{\mathcal{A}})$ at receiver transverse coordinates r distributed uniformly in $\mathcal{A}$ at distance $0.095\lambda_c$ apart. We compute $p(t, r, z_{\mathcal{A}})$ in the time window $t \in (130, 333)$ms, which contains the direct arrival at $\tau = z_{\mathcal{A}}/c_o = 164.7$ms and the arrival of sufficiently many other guided modes after that. The time sampling is at the rate of 15μs.

We show in Figure 3.2 the time trace of $p(t, r = X/2, z_{\mathcal{A}})$ for the source at $x_\star = X/2$ and various perturbation parameters ε. The picture on the top left is in the unperturbed waveguide ($\varepsilon = 0$). Since the source emits a short pulse $\varphi(t)$, we can clearly distinguish the arrival of the modes at the array. In the perturbed waveguide, we note the significant effect on the traces of scattering by the random inhomogeneities, especially in the cases $\varepsilon = 2\%$ and 3%. This is the regime we are interested in, where the random fluctuations cause strong mode coupling and the array data is almost incoherent.

3.1. Numerical results. We illustrate the performance of the three coherent imaging functions $\mathcal{I}(\vec{x}^s)$, $\mathcal{I}^{MF}(\vec{x}^s)$, and $\mathcal{I}^{CINT}(\vec{x}^s)$ in Figures 3.3–3.6. The source

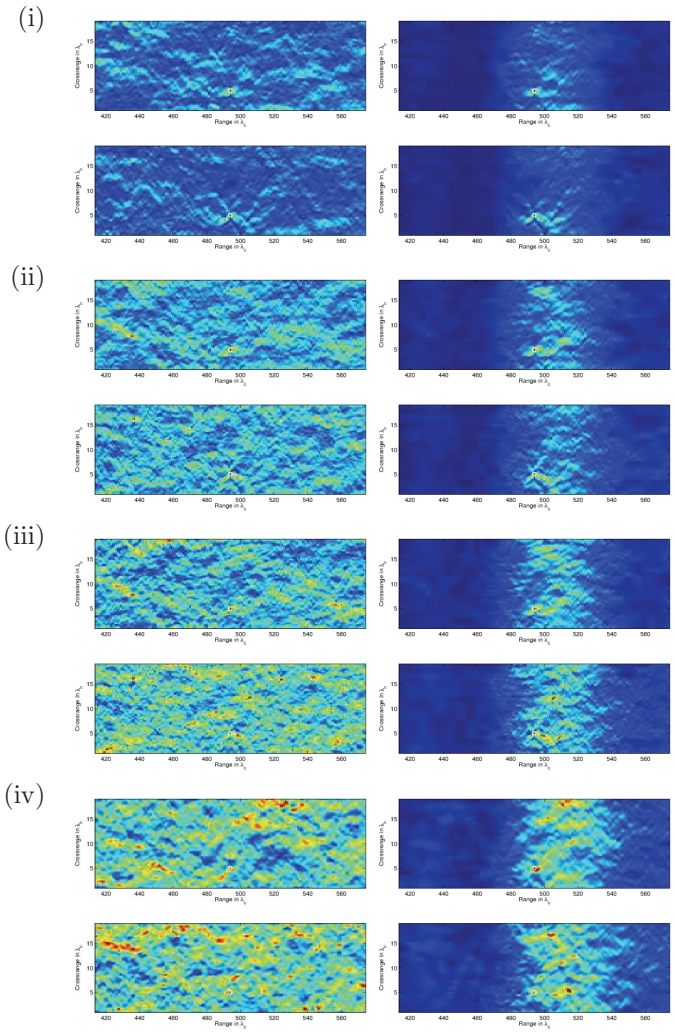

FIG. 3.4. *Left column:* $\mathcal{I}^{MF}(\vec{x}^s)$ *for two realizations of the random medium. Right column:* $\mathcal{I}^{CINT}(\vec{x}^s)$. *The plots are for* $x_\star = X/4$, $\varepsilon = 2\%$ *in* (i)–(iii), *and* $\varepsilon = 3\%$ *in* (iv). *The central frequency is* $2.69kHz$ *in* (i), $2.99kHz$ *in* (ii), $3.13kHz$ *in* (iii), *and* $2.09kHz$ *in* (iv). *The bandwidth is* $0.375kHz$. *The CINT images are computed with* $\Omega_d = 0.045kHz$. *The abscissa is range in* λ_c, *and the ordinate is cross-range in* λ_c.

is at cross-range coordinate $x_\star = X/4 = 5\lambda_c$. All the methods work well for weak fluctuations $\varepsilon \leq 1\%$, so we do not show the images here. The results in Figure 3.3 are for $\varepsilon = 2\%$, central frequency $\omega_o/(2\pi) = 2.09$kHz, and bandwidth $\varepsilon B/(2\pi) = 0.375$kHz, that is, $B \approx 9\omega_o$. We show the images for two realizations of the random medium. Both matched field and CINT locate the source correctly, and the images do not change significantly from one realization to another. Function $\mathcal{I}(\vec{x}^s)$ does not behave as well, and we start to see its statistical instability.

Figure 3.4 illustrates how both matched field and CINT deteriorate as the data loses its coherence. The progressive loss of coherence occurs as we increase the central frequency ω_o and the scaled range $Z = \varepsilon^2 z_{\mathcal{A}}$. In our case $z_{\mathcal{A}}$ is fixed at $494\lambda_c$, so we increase Z by increasing ε. We note in Figure 3.4 that matched field and CINT

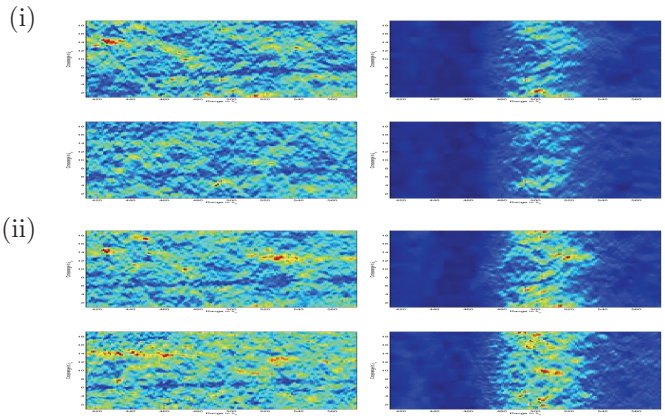

FIG. 3.5. *Left column:* $\mathcal{I}^{MF}(\vec{x}^s)$ *for two realizations of the random medium. Right column:* $\mathcal{I}^{CINT}(\vec{x}^s)$. *We take* $x_\star = X/4$, $\varepsilon = 2\%$, *central frequency* $2.69kHz$, *and bandwidth* $0.375kHz$. *In* (i) *the aperture is* $\mathcal{A} = [0, 12\lambda_c]$ *and in* (ii) $\mathcal{A} = [0, 8\lambda_c]$. *The CINT images are computed with* $\Omega_d = 0.045kHz$. *The abscissa and ordinate are range and cross-range in* λ_c.

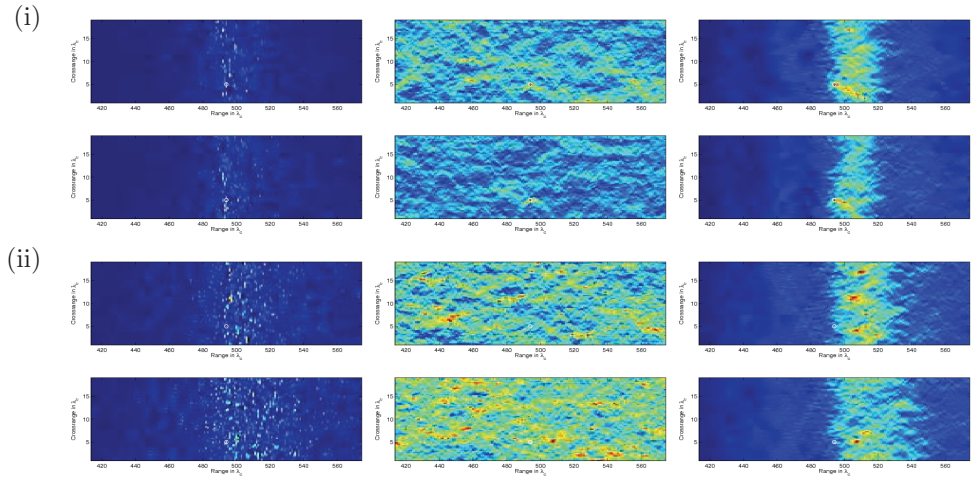

FIG. 3.6. *From left to right:* $\mathcal{I}(\vec{x}^s)$, $\mathcal{I}^{MF}(\vec{x}^s)$, *and* $\mathcal{I}^{CINT}(\vec{x}^s)$ *for the source at* $x_\star = X/4$, *full aperture, and the extra wide band signal* $\varphi(t)$, *with bandwidth* 1.5–$4.5kHz$. *In* (i) *we show two realizations at* $\varepsilon = 2\%$. *In* (ii) *we show two realizations at* $\varepsilon = 3\%$. *The CINT images are computed with* $\Omega_d = 0.09kHz$. *The abscissa and ordinate are range and cross-range in* λ_c.

locate the source correctly, in both realizations of the random medium, at $\varepsilon = 2\%$ and $\omega_o/(2\pi) = 2.69$kHz (case (i)). However, as ω_o increases, both methods deteriorate (cases (ii)–(iii)). Matched field gives no range resolution, and there are many spurious peaks. There are spurious peaks in the CINT images too, although they have some range information. The results are even worse in case (iv), where we increase ε to 3%.

The images in Figures 3.3 and 3.4 are at full aperture $\mathcal{A} = [0, X]$. The results are naturally worse for partial apertures, as seen in Figure 3.5 for the same bandwidth as in case (i) in Figure 3.4 and partial apertures $\mathcal{A} = [0, 12\lambda_c]$ and $\mathcal{A} = [0, 8\lambda_c]$, respectively.

Finally, we show in Figure 3.6 the images obtained with all three coherent source localization functions for fluctuations $\varepsilon = 2\%$ and $\varepsilon = 3\%$, full aperture, and the

entire extra wide band of 1.5–4.5kHz. We note that the extra wide band does not help much in the source localization, especially at $\varepsilon = 3\%$.

3.2. Summary of the results. The numerical results in Figures 3.3–3.6 show the progressive degradation of the performance of coherent source localization methods in random waveguides. When wave scattering is weak, the methods work well. As we increase ε (i.e., the scaled range Z) and the central frequency ω_o, the random inhomogeneities have a stronger and stronger cumulative effect, and the wave field at the array loses its coherence. Consequently, none of the coherent methods works, although CINT appears slightly better because it gives some range information. Nevertheless, the CINT range resolution is very poor, over an interval of order $50\lambda_c$, which is not centered at the correct range $z_{\mathcal{A}}$. We explain this behavior with analysis in section 5, where we show that wave scattering causes a strong dispersive effect that is not accounted for in the back propagation in CINT.

In order to localize the source at very long ranges, with almost incoherent array data, we need to systematically exploit the dispersive effect induced by the random inhomogeneities. This requires a mathematical model that allows us to cast the source localization problem as one of parameter estimation for the source coordinates and possibly the statistics of the random fluctuations. Such a model was derived in [14, 9, 12, 11]. We use it in section 6 to formulate and analyze our incoherent source localization method.

4. Mathematical model of the waveguide. In an ideal waveguide, the sound speed varies only in the transverse direction and energy is transmitted by guided modes, the orthogonal eigenfunctions of the symmetric differential operator $\partial_x^2 + \omega^2/c^2$. Then, $\widehat{p}(\omega, \vec{x})$ is given by a mode expansion using separation of variables in (2.6).

We consider waveguides with weak random inhomogeneities and model the sound speed as

$$\frac{c_o^2}{c^2(\vec{x})} = \begin{cases} 1 + \varepsilon\nu(\vec{x}), & z \in \left[0, L/\varepsilon^2\right], \\ 1, & z \in (-\infty, 0) \cup \left(L/\varepsilon^2, \infty\right). \end{cases} \tag{4.1}$$

Here $\varepsilon \ll 1$ is the perturbation parameter and $\nu(\vec{x})$ is a bounded mean zero random process, stationary and ergodic in z, with enough long range decorrelation,[1] as stated in technical terms in [17, section 4.6.2]. We write that the fluctuations are supported in the rectangle $[0, X] \times [0, L/\varepsilon^2]$ because we consider very long ($\sim \varepsilon^{-2}$) distances of propagation to get strong scattering effects. If we observe $p(t, \vec{x})$ for time $t \leq \tau/\varepsilon^2$, we obtain by the causality of the wave equation that it is not influenced by the medium beyond range L/ε^2, with $L \approx c_o\tau$, so we may as well assume a uniform sound speed for $z > L/\varepsilon^2$. The bound $z = 0$ on the support of the fluctuations may be motivated by the forward scattering approximation. It is shown in [14, 9, 12, 11] that the statistical coupling between the forward and backward going modes is negligible when the random fluctuations are not too rough, that is, if the autocorrelation of $\nu(\vec{x})$ is smooth enough in z. Then, we can neglect the waves scattered to the left of the source, as if we had an unperturbed medium for $z < 0$.

4.1. The pressure field in unperturbed waveguides. Note that in (4.1) we take a uniform background speed c_o to simplify the analysis and obtain frequency

[1] This technical assumption is needed later to apply averaging methods for stochastic differential equations [11, Chapter 6].

independent modes $\phi_j(x)$ in the unperturbed waveguide

$$-\frac{d^2\phi_j(x)}{dx^2} = \mu_j\phi_j(x), \qquad x \in (0,X),$$
$$\phi_j(0) = \phi_j(X) = 0, \qquad j = 1,2,\ldots. \tag{4.2}$$

The theory can be carried out for variable backgrounds $c_o = c_o(x)$ [14, 9] with some slight complications induced by the frequency dependence of the eigenvalues and eigenfunctions of $\frac{\partial^2}{\partial x^2} + \frac{\omega^2}{c_o^2(x)}$.

In the constant background case we have

$$\phi_j(x) = \sqrt{\frac{2}{X}}\sin\left(\frac{\pi j x}{X}\right), \quad \mu_j = \left(\frac{\pi j}{X}\right)^2, \quad j = 1,2\ldots, \tag{4.3}$$

and the pressure field in the unperturbed waveguide is given by

$$p_o(t,\vec{x}) = \int \frac{d\omega}{2\pi}\widehat{p}_o(\omega,\vec{x})e^{-i\omega t}, \tag{4.4}$$

with Fourier coefficients [11]

$$\widehat{p}_o(\omega,\vec{x}) = \frac{\widehat{f}(\omega)}{2}\left[\sum_{j=1}^{N(\omega)}\phi_j(x_\star)\phi_j(x)e^{i\beta_j(\omega)z} + \sum_{j>N(\omega)}\phi_j(x_\star)\phi_j(x)e^{-\beta_j(\omega)z}\right] \tag{4.5}$$

and for $z > 0$. Here $\beta_j(\omega)$ are the modal wavenumbers

$$\beta_j(\omega) = \begin{cases} \sqrt{\left(\frac{2\pi}{\lambda}\right)^2 - \mu_j}, & j = 1,2,\ldots,N(\omega), \\ \sqrt{\mu_j - \left(\frac{2\pi}{\lambda}\right)^2}, & j > N(\omega), \end{cases} \tag{4.6}$$

$\lambda = 2\pi c_o/\omega$ is the wavelength, and $N(\omega) = \left\lfloor \frac{2X}{\lambda} \right\rfloor$ is the number of propagating modes, defined as the largest integer satisfying $\mu_{N(\omega)} \le (2\pi/\lambda)^2$. The modes indexed by $j > N(\omega)$ are evanescent.

4.2. The pressure field in random waveguides. The Fourier coefficients $\widehat{p}(\omega,\vec{x})$ of the random pressure field can be written as an expansion in the unperturbed eigenfunctions, with random amplitudes a_j and b_j of the forward and backward propagating modes and random amplitudes $\mathcal{E}_j$ of the evanescent modes [11, section 20.2.1]:

$$\widehat{p}(\omega,\vec{x}) = \widehat{f}(\omega)\left\{\sum_{j=1}^{N(\omega)}\left[\frac{a_j(\omega,z)}{\sqrt{\beta_j(\omega)}}\phi_j(x)e^{i\beta_j(\omega)z} + \frac{b_j(\omega,z)}{\sqrt{\beta_j(\omega)}}\phi_j(x)e^{-i\beta_j(\omega)z}\right]\right.$$
$$\left. + \sum_{j>N(\omega)}\mathcal{E}_j(\omega,z)\phi_j(x)\right\}. \tag{4.7}$$

Here $z > 0$, and we now scale it as $z \rightsquigarrow z/\varepsilon^2$ to get significant coupling of the modes by cumulative scattering in the random medium over very long ranges.

After some algebraic manipulations detailed in [11, section 20.2.4], involving the projection of (2.6) on $\phi_j(x)$, and expressing the evanescent amplitudes in terms of a_j and b_j, we obtain a system of differential equations

$$\frac{\partial}{\partial z}\begin{bmatrix}\mathbf{a}^\varepsilon(\omega,z)\\ \mathbf{b}^\varepsilon(\omega,z)\end{bmatrix} \approx \left\{\frac{1}{\varepsilon}\mathbb{P}\left(\omega,\frac{z}{\varepsilon^2}\right)+\mathbb{E}\left(\omega,\frac{z}{\varepsilon^2}\right)\right\}\begin{bmatrix}\mathbf{a}^\varepsilon(\omega,z)\\ \mathbf{b}^\varepsilon(\omega,z)\end{bmatrix} \tag{4.8}$$

for the vector valued random processes

$$\begin{aligned}\mathbf{a}^\varepsilon(\omega,z) &= \left(a_1(\omega,z/\varepsilon^2),\ldots,a_{N(\omega)}(\omega,z/\varepsilon^2)\right)^T,\\ \mathbf{b}^\varepsilon(\omega,z) &= \left(b_1(\omega,z/\varepsilon^2),\ldots,b_{N(\omega)}(\omega,z/\varepsilon^2)\right)^T,\end{aligned} \tag{4.9}$$

defined for $z\geq 0$. The source at $z=0$ gives

$$a_j(\omega,0)=a_{o,j}(\omega;x_\star)=\frac{\sqrt{\beta_j(\omega)}}{2}\phi_j(x_\star),\qquad j=1,\ldots,N(\omega), \tag{4.10}$$

and the field is outgoing at the range limit L/ε^2 of the fluctuations, $\mathbf{b}^\varepsilon(\omega,L)=\mathbf{0}$. The forward and backward propagating mode amplitudes are coupled in (4.8) by

$$\mathbb{P}(\omega,z)=\begin{bmatrix}\mathbb{P}^{(a,a)}(\omega,z) & -\mathbb{D}(\omega,z)\overline{\mathbb{P}^{(a,a)}}(\omega,z)\\ -\overline{\mathbb{D}}(\omega,z)\mathbb{P}^{(a,a)}(\omega,z) & \overline{\mathbb{P}^{(a,a)}}(\omega,z)\end{bmatrix} \tag{4.11}$$

and

$$\mathbb{E}(\omega,z)=\begin{bmatrix}\mathbb{E}^{(a,a)}(\omega,z) & -\mathbb{D}(\omega,z)\overline{\mathbb{E}^{(a,a)}}(\omega,z)\\ -\overline{\mathbb{D}}(\omega,z)\mathbb{E}^{(a,a)}(\omega,z) & \overline{\mathbb{E}^{(a,a)}}(\omega,z)\end{bmatrix}, \tag{4.12}$$

where $\mathbb{D}(\omega,z)=\mathrm{diag}\left(e^{-2i\beta_1(\omega)z},\ldots,e^{-2i\beta_{N(\omega)}(\omega)z}\right)$. The $N(\omega)\times N(\omega)$ matrix $\mathbb{P}^{(a,a)}$ in the leading coupling term is given by

$$\mathbb{P}^{(a,a)}_{jl}(\omega,z)=\frac{i\omega^2}{2c_o^2}\frac{C_{jl}(z)}{\sqrt{\beta_j(\omega)\beta_l(\omega)}}e^{i[\beta_l(\omega)-\beta_j(\omega)]z} \tag{4.13}$$

in terms of the random stationary processes

$$C_{jl}(z)=\int_0^X \nu(x,z)\phi_j(x)\phi_l(x)dx,\qquad j,l=1,2,\ldots. \tag{4.14}$$

The second order coupling in (4.8) is via the evanescent modes through the matrix

$$\mathbb{E}^{(a,a)}_{jl}(\omega,z)=\frac{i\omega^4}{4c_o^4}\sum_{l'>N(\omega)}\int_{-\infty}^{\infty}ds\frac{C_{jl'}(z)C_{ll'}(z+s)}{\beta_{l'}(\omega)\sqrt{\beta_j(\omega)\beta_l(\omega)}}e^{i\beta_l(\omega)(z+s)-i\beta_j(\omega)z-\beta_{l'}(\omega)|s|}. \tag{4.15}$$

4.2.1. The forward scattering approximation. It follows from the diffusion approximation theorem [11, section 6.5] applied to (4.8) that $(\mathbf{a}^\varepsilon(\omega,z),\mathbf{b}^\varepsilon(\omega,z))$ can be identified in the limit $\varepsilon\to 0$ with a diffusion process in $\mathbb{C}^{2N(\omega)}$, solving a system of linear stochastic differential equations [11, section 20.3]. Assuming a smooth correlation function of the random stationary processes (4.14) (i.e., z-autocorrelation of $\nu(\vec{x})$), the coupling between the forward and backward propagating modes becomes

negligible as $\varepsilon \to 0$, and we can make the forward scattering approximation [11, section 20.2.6]

$$\frac{\partial}{\partial z}\mathbf{a}^\varepsilon(\omega,z) = \left[\frac{1}{\varepsilon}\mathbb{P}^{(a,a)}\left(\omega,\frac{z}{\varepsilon^2}\right) + \mathbb{E}^{(a,a)}\left(\omega,\frac{z}{\varepsilon^2}\right)\right]\mathbf{a}^\varepsilon(\omega,z), \qquad z>0,$$

$$\mathbf{a}^\varepsilon(\omega,0) = \mathbf{a}_o(\omega;x_\star) = \left(a_{o,1}(\omega;x_\star),\ldots,a_{o,N(\omega)}(\omega;x_\star)\right)^T. \tag{4.16}$$

Since the stochastic differential equations (4.16) are linear, we write

$$\mathbf{a}^\varepsilon(\omega,z) = T^\varepsilon(\omega,z)\mathbf{a}_o(\omega;x_\star), \tag{4.17}$$

using the random $N(\omega)\times N(\omega)$ transfer matrix $T^\varepsilon(\omega,z)$, the fundamental solution of (4.16). It satisfies the stochastic system of differential equations

$$\frac{\partial}{\partial z}T^\varepsilon(\omega,z) = \left[\frac{1}{\varepsilon}\mathbb{P}^{(a,a)}\left(\omega,\frac{z}{\varepsilon^2}\right) + \mathbb{E}^{(a,a)}\left(\omega,\frac{z}{\varepsilon^2}\right)\right]T^\varepsilon(\omega,z), \qquad z>0, \tag{4.18}$$

and the initial condition

$$T^\varepsilon(\omega,0) = I, \tag{4.19}$$

with I the identity matrix.

4.2.2. Mathematical model of the array data. Let $(r, z_{\mathcal{A}} = Z/\varepsilon^2)$ be the receiver coordinates, with r taking values in the array aperture $\mathcal{A} \subseteq [0,X]$. The mathematical model of the array data is

$$p^\varepsilon(t,r,Z) = \int \frac{d\omega \widehat{f}^\varepsilon(\omega)}{4\pi}\sum_{j,l=1}^{N(\omega)}\sqrt{\frac{\beta_l(\omega)}{\beta_j(\omega)}}T^\varepsilon_{jl}(\omega,Z)\phi_j(r)\phi_l(x_\star)e^{-i\omega t + i\beta_j(\omega)Z/\varepsilon^2}, \tag{4.20}$$

where $p^\varepsilon(t,r,Z) = p(t,r,Z/\varepsilon^2)$ and we renamed as $\widehat{f}^\varepsilon(\omega)$ the Fourier coefficients of the pulse. To study the role of the bandwidth on the focusing and statistical stability of source localization, we scale the bandwidth relative to ε at central frequency ω_o and define

$$\widehat{f}^\varepsilon(\omega) = \frac{1}{\varepsilon^\sigma}\widehat{f}_B\left(\frac{\omega-\omega_o}{\varepsilon^\sigma}\right) \tag{4.21}$$

for $\sigma \le 2$. The Fourier transform $\widehat{f}_B$ of the base band pulse f_B is supported in $[-B,B]$, and the time support of the source signal

$$f^\varepsilon(t) = \int \frac{d\omega}{2\pi}\widehat{f}^\varepsilon(\omega)e^{-i\omega t} = e^{-i\omega_o t}f_B(\varepsilon^\sigma t) \tag{4.22}$$

is $\sim \varepsilon^{-\sigma}/B$. As we mentioned in section 3, in the *narrow band* case ($\sigma = 2$) $f^\varepsilon(t)$ is spread out over a long time, comparable to the travel time $\varepsilon^{-2}Z/c_o$. The support of $f^\varepsilon(t)$ is much smaller than the travel time in *broad band* cases ($\sigma < 2$), so that we can distinguish at the array a train of pulses corresponding to arrivals of different modes.

We restrict our study to $\sigma \in (1,2]$. This choice is convenient in the analysis because we can freeze the number of propagating modes in (4.20) to $N(\omega_o)$ and obtain the simpler model

$$p^\varepsilon(t,r,Z) \approx \frac{1}{4\pi}\sum_{j,l=1}^{N(\omega_o)}\sqrt{\frac{\beta_l(\omega_o)}{\beta_j(\omega_o)}}\phi_j(r)\phi_l(x_\star)\int d\omega\, \widehat{f}^\varepsilon(\omega)\, T^\varepsilon_{jl}(\omega,Z)\, e^{-i\omega t + i\beta_j(\omega)Z/\varepsilon^2}, \tag{4.23}$$

with phase given by

$$\beta_j(\omega_o+\varepsilon^\sigma h)\frac{Z}{\varepsilon^2}\approx\beta_j(\omega_o)\frac{Z}{\varepsilon^2}+h\beta_j'(\omega_o)\frac{Z}{\varepsilon^{2-\sigma}}. \tag{4.24}$$

In the case $\sigma=1$, the phase has the extra dispersive term $h^2/2\beta_j''(\omega_o)Z$. The ultrawide bandwidth case $\sigma<1$ is a bit more tedious to analyze, and it does not improve the images, as seen in Figure 3.6.

Although the array has finitely many receivers, we assume from now on that their spacing h_r is small, so that the sums $\sum_{r\in\mathcal{A}}$ appearing in the expression of the imaging functions approximate the scaled integrals $h_r^{-1}\int_{\mathcal{A}}dr$. Since the integrands involve the eigenfunctions $\phi_j(r)$, the continuum aperture approximation made in this paper is valid for receiver spacings h_r that are small enough to capture the oscillations of the highest frequency modes used in the imaging functions. A complete analysis of the role played by the density of the array sensors in the imaging process involves signal-to-noise ratio (SNR) issues. It is expected that denser arrays give better results in the presence of additive, ambient noise. In this paper we do not consider such SNR analysis, and we concentrate solely on the random medium effects on the imaging process.

5. Coherent source localization methods. We give here a detailed analysis of the deterioration of the coherent source localization methods illustrated with numerical simulations in section 3.1. The analysis uses data model (4.23) to estimate the mean and variance of the source localization functions in the asymptotic limit $\varepsilon\to 0$. The mean shows how the images are expected to focus. The variance determines the statistical stability of the methods with respect to the realizations of the fluctuations of the wave speed.

5.1. Back propagation in homogeneous waveguides. The Green's function of Helmholtz's equation in the unperturbed waveguide, for a hypothetical source at $\vec{x}^s=(x^s,z^s)$, is given by

$$\widehat{G}_o(\omega,x,z;\vec{x}^s)\approx\frac{1}{2}\sum_{j=1}^{N(\omega)}\phi_j(x^s)\phi_j(x)e^{i\beta_j(\omega)(z-z^s)} \tag{5.1}$$

at large $z-z^s$, where the evanescent modes can be neglected. The source localization function follows from (2.7), in the continuum aperture approximation, after scaling with the distance between the receivers:

$$\begin{aligned}\mathcal{I}(\vec{x}^s)&=\int\frac{d\omega}{2\pi}\int_{\mathcal{A}}dr\,\overline{\widehat{p}}(\omega,r,z_{\mathcal{A}})\widehat{G}_o(\omega,r,z_{\mathcal{A}};\vec{x}^s)\\ &\approx\frac{1}{2}\sum_{j=1}^{N(\omega_0)}\phi_j(x^s)\int\frac{d\omega}{2\pi}\,e^{i\beta_j(\omega)(z_{\mathcal{A}}-z^s)}\int_{\mathcal{A}}dr\,\phi_j(r)\overline{\widehat{p}}(\omega,r,z_{\mathcal{A}}).\end{aligned} \tag{5.2}$$

5.1.1. Unperturbed waveguides. When the waveguide is indeed homogeneous, $\widehat{p}$ is the same as $\widehat{p}_o$ given by (4.5), and $\mathcal{I}(\vec{x}^s)$ becomes the time reversal function

$$\mathcal{I}_o^{TR}(\vec{x}^s)\approx\frac{1}{4}\sum_{j,l=1}^{N(\omega_o)}\mathcal{M}_{jl}\,\phi_j(x_\star)\phi_l(x^s)\int\frac{d\omega}{2\pi}\overline{\widehat{f^\varepsilon}}(\omega)e^{i\beta_l(\omega)Z^s/\varepsilon^2-i\beta_j(\omega)Z/\varepsilon^2}. \tag{5.3}$$

Here we recalled the long range scaling $z_{\mathcal{A}} = Z/\varepsilon^2$ and let $z_{\mathcal{A}} - z^s = Z^s/\varepsilon^2$, with Z^s of order one. We also introduced matrix

$$\mathcal{M}_{jl} = \int_{\mathcal{A}} \phi_j(r)\phi_l(r)dr, \tag{5.4}$$

depending on the aperture $\mathcal{A}$. In the ideal full aperture case, $\mathcal{M}$ is the identity by the orthonormality of the eigenfunctions $\phi_j(x)$. For partial apertures, with $\mathcal{A}$ proper subsets of $[0, X]$, $\mathcal{M}$ couples the modes in (5.3).

Naturally, the best source localization is for a full aperture:

$$\begin{aligned}\mathcal{I}_o^{TR}(\vec{x}^s) &\approx \frac{1}{4}\sum_{j=1}^{N(\omega_o)} \phi_j(x_\star)\phi_j(x^s) \int \frac{d\omega}{2\pi\varepsilon^\sigma}\overline{\widehat{f}_B}\left(\frac{\omega-\omega_o}{\varepsilon^\sigma}\right) e^{i\beta_j(\omega)(Z^s-Z)/\varepsilon^2} \\ &\approx \frac{1}{4}\sum_{j=1}^{N(\omega_o)} \phi_j(x_\star)\phi_j(x^s) e^{i\beta_j(\omega_o)(Z^s-Z)/\varepsilon^2}\overline{f_B}\left(\beta_j'(\omega_o)\frac{Z^s-Z}{\varepsilon^{2-\sigma}}\right). \end{aligned} \tag{5.5}$$

We show in Appendix A that $\mathcal{I}_o^{TR}(\vec{x}^s)$ focuses at $\vec{x}_\star = (x_\star, 0)$. Because of the $O(1)$ support of the carrier pulse f_B, each term in (5.5) peaks at search ranges z^s satisfying $|z^s| = |Z - Z^s|/\varepsilon^2 \le O(\varepsilon^{-\sigma}\lambda_o)$. However, $\mathcal{I}_o^{TR}$ has much better range resolution, due to the rapid phase in (5.5) and the summation over the modes. Explicitly, we show in Appendix A that for a large enough number $N(\omega_o)$ of modes

$$\mathcal{I}_o^{TR}(x^s = x_\star, z^s) \approx \frac{1}{4}\sum_{j=1}^{N(\omega_o)} \phi_j^2(x_\star) e^{i\beta_j(\omega_o)(Z^s-Z)/\varepsilon^2}\overline{f_B}\left(\beta_j'(\omega_o)\frac{Z^s-Z}{\varepsilon^{2-\sigma}}\right)$$

focuses with range resolution $O(\lambda_o)$. Furthermore,

$$\mathcal{I}_o^{TR}(x^s, z^s = 0) \approx \frac{\overline{f_B}(0)}{2\lambda_o}\,\mathrm{sinc}\left[\frac{2\pi(x^s - x_\star)}{\lambda_o}\right] \tag{5.6}$$

has cross-range resolution (distance from the peak to the first zero) equal to the diffraction limit $\lambda_o/2$.

5.1.2. Random waveguides. As noted in section 2.1, (5.2) is not the same as time reversal in random waveguides, because the back propagation is synthetic, via the unperturbed Green's function $\widehat{G}_o$. Time reversal works well in random waveguides [12, 16], but it cannot be used for source localization. Moreover, the back propagation in the fictitious unperturbed waveguide does not work well, as illustrated in section 3.1 and as follows from the analysis below.

Let us present for simplicity only the full aperture case. The results are worse for partial apertures, as seen in Figure 3.5. Using model (4.23) in (5.2), we get

$$\mathcal{I}(\vec{x}^s) \approx \frac{1}{4}\sum_{j,l=1}^{N(\omega_o)} \sqrt{\frac{\beta_l(\omega_o)}{\beta_j(\omega_o)}}\phi_j(x^s)\phi_l(x_\star)\int \frac{dh}{2\pi}\overline{\widehat{f}_B}(h)\,\overline{T_{jl}^\varepsilon}(\omega_o+\varepsilon^\sigma h, Z)e^{i\beta_j(\omega_o+\varepsilon^\sigma h)\frac{(Z^s-Z)}{\varepsilon^2}}. \tag{5.7}$$

This is a randomly fluctuating function, with modes coupled by the transfer matrix T_{jl}^ε, and we estimate its expectation and variance for $\varepsilon \ll 1$ and $\sigma \in (1, 2)$. The statistical stability is worse in the narrow band case $\sigma = 2$.

5.1.3. The statistical mean. To estimate $E\{\mathcal{I}(\vec{x}^s)\}$, we recall the relevant results from [11, section 20.3], summarized in the following lemma.

LEMMA 5.1. *In the asymptotic limit $\varepsilon \to 0$, the expectation of the transfer matrix is given by*

$$\lim_{\varepsilon\to 0} E\left\{T^{\varepsilon}_{jl}(\omega, Z)\right\} = \delta_{jl}\, e^{-\mathcal{D}_j(\omega)Z + i\mathcal{O}_j(\omega)Z}, \tag{5.8}$$

where δ_{jl} is the Kronecker delta symbol and $\mathcal{D}_j(\omega)$, $\mathcal{O}_j(\omega)$ are parameters dependent on the frequency and correlation function of the fluctuations. Explicitly,

$$\mathcal{D}_j(\omega) = \left[\Gamma^{(1)}_{jj}(\omega) - \Gamma^{(c)}_{jj}(\omega)\right]/2, \qquad \mathcal{O}_j(\omega) = \Gamma^{(s)}_{jj}(\omega)/2 + \kappa_j(\omega), \tag{5.9}$$

where

$$\Gamma^{(c)}_{jl}(\omega) = \frac{\omega^4}{4c_o^4\beta_j(\omega)\beta_l(\omega)} \int_{-\infty}^{\infty} \cos\left[(\beta_j(\omega) - \beta_l(\omega))\, z\right] E\left\{C_{jl}(0)C_{jl}(z)\right\} dz, \quad j \neq l,$$

$$\Gamma^{(c)}_{jj}(\omega) = -\sum_{l'\neq j,\, l'=1}^{N(\omega)} \Gamma^{(c)}_{jl'}(\omega), \tag{5.10}$$

$$\Gamma^{(s)}_{jl}(\omega) = \frac{\omega^4}{4c_o^4\beta_j(\omega)\beta_l(\omega)}\, 2\int_{0}^{\infty} \sin\left[(\beta_j(\omega) - \beta_l(\omega))\, z\right] E\left\{C_{jl}(0)C_{jl}(z)\right\} dz, \quad j \neq l,$$

$$\Gamma^{(s)}_{jj}(\omega) = -\sum_{l'\neq j,\, l'=1}^{N(\omega)} \Gamma^{(s)}_{jl'}(\omega), \tag{5.11}$$

$$\Gamma^{(1)}_{jl}(\omega) = \frac{\omega^4}{4c_o^4\beta_j(\omega)\beta_l(\omega)} \int_{-\infty}^{\infty} E\left\{C_{jj}(0)C_{ll}(z)\right\} dz \quad \textit{for all } j, l, \tag{5.12}$$

$$\kappa_j(\omega) = \sum_{l'>N(\omega)} \frac{\omega^4}{4c_o^4\beta_j(\omega)\beta_{l'}(\omega)} \int_{-\infty}^{\infty} E\left\{C_{jl'}(0)C_{jl'}(z)\right\} \cos\left(\beta_j(\omega)z\right) e^{-\beta_{l'}(\omega)|z|} dz, \tag{5.13}$$

and $j, l = 1, \ldots, N(\omega)$.

Note that coefficients $\Gamma^{(c)}_{jl}(\omega)$ are nonnegative for $j \neq l$ by Bochner's theorem because they are proportional to the power spectral densities of the stationary random process $C_{jl}(z)$ given by (4.14). Therefore, $\Gamma^{(c)}_{jj}(\omega) < 0$. Similarly, $\Gamma^{(1)}_{jj}(\omega)$ are nonnegative since they are proportional to the power spectral densities of $C_{jj}(z)$ evaluated at a zero dual argument to z. Thus, $\mathcal{D}_j(\omega) > 0$ and the expectation in (5.9) decays exponentially with Z and ω. This decay means that the wave field loses its coherence rapidly, and the energy is transferred to the random (incoherent) fluctuations. Coefficients $\mathcal{O}_j(\omega)$ account for the dispersive effect of the random medium on the mean field. Dispersion is induced by coupling of the propagating modes ($\Gamma^{(s)}_{jl}(\omega)$) and by coupling with the evanescent modes ($\kappa_j(\omega)$).

The expectation of (5.7) becomes

$$E\left\{\mathcal{I}(\vec{x}^s)\right\} \approx \frac{1}{4}\sum_{j=1}^{N(\omega_o)} \phi_j(x^s)\phi_j(x_\star) e^{-[\mathcal{D}_j(\omega_o) - i\mathcal{O}_j(\omega_o)]Z + i\beta_j(\omega_o)\frac{(Z^s - Z)}{\varepsilon^2}}$$
$$\times\, \overline{f_B}\left(\beta_j'(\omega_o)(Z^s - Z)/\varepsilon^{2-\sigma}\right). \tag{5.14}$$

It is similar to (5.5), except for the exponential damping and the oscillations caused by the random medium. This does not affect the range focus, which is almost the

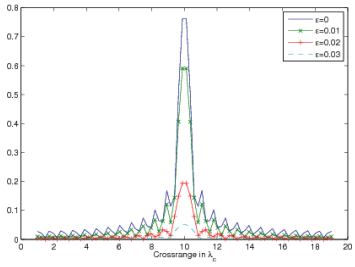

FIG. 5.1. $E\{\mathcal{I}(x^s,0)\}$ *for the source at* $x_\star = X/2 = 10\lambda_c$ *and various* ε.

same as in section 5.1. We plot[2] in Figure 5.1 $E\{\mathcal{I}(x^s,0)\}$, and note that it peaks at $x_\star$, but the peak value decreases rapidly (exponentially) as we increase ε, that is, as we increase Z. The exponential decay of $E\{\mathcal{I}(\vec{x}_\star)\}$ is also captured by the upper bound

$$|E\{\mathcal{I}(\vec{x}_\star)\}| \le \frac{|f_B(0)|}{4} e^{-\mathcal{D}_{\min}(\omega_o)Z} \sum_{j=1}^{N(\omega_o)} \phi_j^2(x_\star) \approx \frac{C|f_B(0)|}{\lambda_o} e^{-\mathcal{D}_{\min}(\omega_o)Z}, \tag{5.15}$$

where C is an $O(1)$ constant, and $\mathcal{D}_{\min}(\omega_o) = \min_{j=1,\dots,N(\omega_o)} \mathcal{D}_j(\omega_o)$.

5.1.4. The variance. Now, let us compute the variance

$$V(\vec{x}_\star) = E\left\{|\mathcal{I}(\vec{x}_\star)|^2\right\} - |E\{\mathcal{I}(\vec{x}_\star)\}|^2$$

at the peak $\vec{x}^s = \vec{x}_\star$ of $E\{\mathcal{I}(\vec{x}^s)\}$. It is given by

$$\begin{aligned} V(\vec{x}_\star) \approx \frac{1}{16} \sum_{j,l,j',l'=1}^{N(\omega_o)} & \sqrt{\frac{\beta_l(\omega_o)\beta_{l'}(\omega_o)}{\beta_j(\omega_o)\beta_{j'}(\omega_o)}} \phi_j(x_\star)\phi_l(x_\star)\phi_{j'}(x_\star)\phi_{l'}(x_\star) \int \frac{dh}{2\pi} \int \frac{dh'}{2\pi} \overline{\widehat{f}_B}(h)\widehat{f}_B(h') \\ & \times \Big[E\left\{ T^\varepsilon_{jl}(\omega_o + \varepsilon^\sigma h, Z)\overline{T^\varepsilon_{j'l'}}(\omega_o + \varepsilon^\sigma h', Z)\right\} \\ & - E\left\{T^\varepsilon_{jl}(\omega_o + \varepsilon^\sigma h, Z)\right\} E\left\{\overline{T^\varepsilon_{j'l'}}(\omega_o + \varepsilon^\sigma h', Z)\right\}\Big], \end{aligned} \tag{5.16}$$

so we need two frequency second moments of the transfer matrix in the limit $\varepsilon \to 0$. They are given in [11, Proposition 20.7], and we repeat them in the next lemma.

LEMMA 5.2. *The transfer matrix decorrelates rapidly in frequency:*

$$E\left\{T^\varepsilon_{jl}(\omega, Z)\overline{T^\varepsilon_{j'l'}}(\omega', Z)\right\} \approx E\left\{T^\varepsilon_{jl}(\omega, Z)\right\} E\left\{\overline{T^\varepsilon_{j'l'}}(\omega', Z)\right\} \quad \text{for } |\omega - \omega'|/\omega_o > O(\varepsilon^2). \tag{5.17}$$

At two nearby frequencies,

$$\begin{aligned} \lim_{\varepsilon\to 0} E\left\{T^\varepsilon_{jl}(\omega, Z)\overline{T^\varepsilon_{j'l'}}(\omega - \varepsilon^2 h, Z)\right\} &= \delta_{jj'}\delta_{ll'} \int \mathcal{W}^{(l)}_j(\omega, \tau, Z) e^{ih\left[\tau - \beta'_j(\omega)Z\right]} d\tau \\ &+ (1 - \delta_{jj'})\,\delta_{jl}\delta_{j'l'} e^{-\left[\mathcal{D}_j(\omega) + \mathcal{D}_{j'}(\omega) - \Gamma^{(1)}_{jj'}(\omega)\right]Z + i\left[\mathcal{O}_j(\omega) - \mathcal{O}_{j'}(\omega)\right]Z}, \end{aligned} \tag{5.18}$$

[2]The plots are for the setup described in section 3, with the source at $x_\star = X/2$. The central frequency is at 2.09kHz, and the unscaled bandwidth is 0.375kHz. Note that $z_{\mathcal{A}}$ is fixed at $494\lambda_c$, and therefore a larger ε amounts to a larger scaled Z.

where the Wigner transform $\left\{\mathcal{W}_j^{(l)}(\omega,\tau,z)\right\}_{j=1,\dots,N(\omega)}$ *solves the system of transport equations*

$$\left[\frac{\partial}{\partial z}+\beta_j'(\omega)\frac{\partial}{\partial \tau}\right]\mathcal{W}_j^{(l)}(\omega,\tau,z)=\sum_{n\neq j}\Gamma_{jn}^{(c)}(\omega)\left[\mathcal{W}_n^{(l)}(\omega,\tau,z)-\mathcal{W}_j^{(l)}(\omega,\tau,z)\right] \tag{5.19}$$

for $z>0$*, with initial condition* $\mathcal{W}_j^{(l)}(\omega,\tau,0)=\delta(\tau)\delta_{jl}$*. These solutions are measures,*

$$\mathcal{W}_j^{(l)}(\omega,\tau,Z)=\delta_{jl}\,e^{\Gamma_{ll}^{(c)}(\omega)Z}\delta\left(\tau-\beta_l'(\omega)Z\right)+W_j^{(l)}(\omega,\tau,Z), \tag{5.20}$$

with a Dirac mass at $j=l$ *and continuous density* $W_j^{(l)}(\omega,\tau,Z)$*.*

Because of the $O(\varepsilon^2)$ decoherence frequency, we can restrict the support of the integrals in (5.16) to $|h-h'|\leq \varepsilon^{2-\sigma}\Omega \ll B$ and obtain, after changing variables,

$$\frac{h+h'}{2}\rightsquigarrow h,\qquad h-h'\rightsquigarrow \varepsilon^{2-\sigma}\widetilde{h},$$

that

$$\begin{aligned}V(\vec{x}_\star)\approx\frac{\varepsilon^{2-\sigma}}{4}\sum_{j,l,j',l'=1}^{N(\omega_o)}&\sqrt{\frac{\beta_l(\omega_o)\beta_{l'}(\omega_o)}{\beta_j(\omega_o)\beta_j(\omega_o)}}\phi_j(x_\star)\phi_l(x_\star)\phi_{j'}(x_\star)\phi_{l'}(x_\star)\int_{-B}^{B}\frac{dh}{2\pi}\left|\widehat{f}_B(h)\right|^2\\
&\times\int_{-\Omega}^{\Omega}\frac{d\widetilde{h}}{2\pi}\left[E\left\{T_{jl}^{\varepsilon}\left(\omega_o+\varepsilon^\sigma h+\varepsilon^2\widetilde{h}/2,Z\right)\overline{T_{j'l'}^{\varepsilon}}\left(\omega_o+\varepsilon^\sigma h-\varepsilon^2\widetilde{h}/2,Z\right)\right\}\right.\\
&\left.-E\left\{T_{jl}^{\varepsilon}\left(\omega_o+\varepsilon^\sigma h+\varepsilon^2\widetilde{h}/2,Z\right)\right\}E\left\{\overline{T_{j'l'}^{\varepsilon}}\left(\omega_o+\varepsilon^\sigma h-\varepsilon^2\widetilde{h}/2,Z\right)\right\}\right].\end{aligned}$$

Here we assumed a smooth pulse to make the approximation $\widehat{f}_B(h\pm\varepsilon^{2-\sigma}\widetilde{h}/2)\approx\widehat{f}_B(h)$. The variance follows from Lemmas 5.1 and 5.2, and the continuity in frequency of coefficients (5.9)–(5.13)

$$\begin{aligned}V(\vec{x}_\star)\approx{}&\frac{\varepsilon^{2-\sigma}\|f_B\|^2}{4}\sum_{j,l=1}^{N(\omega_o)}\frac{\beta_l(\omega_o)}{\beta_j(\omega_o)}\phi_j^2(x_\star)\phi_l^2(x_\star)W_j^{(l)}(\omega_o,\beta_j'(\omega_o)Z,Z)\\
&+\frac{\varepsilon^{2-\sigma}\Omega\|f_B\|^2}{4\pi}\sum_{j,j'=1}^{N(\omega_o)}\phi_j^2(x_\star)\phi_{j'}^2(x_\star)\left\{\left[(1-\delta_{jj'})e^{\Gamma_{jj'}^{(1)}(\omega_o)Z}-1\right]\right.\\
&\left.\times e^{-[\mathcal{D}_j(\omega_o)+\mathcal{D}_{j'}(\omega_o)-i\mathcal{O}_j(\omega_o)+i\mathcal{O}_{j'}(\omega_o)]Z}+\delta_{jj'}e^{\Gamma_{jj}^{(c)}(\omega_o)Z}\right\},\end{aligned} \tag{5.21}$$

where

$$\|f_B\|^2=\int\frac{dh}{2\pi}\left|\widehat{f}_B(h)\right|^2=\int dt\,|f_B(t)|^2\,.$$

Note that the second sum in (5.21) is exponentially decaying and negligible at large Z, so we can write

$$V(\vec{x}_\star)\approx\varepsilon^{2-\sigma}\|f_B\|^2\mathcal{F}(\omega_o,Z,x_\star), \tag{5.22}$$

where

$$\mathcal{F}(\omega_o,Z,x_\star)=\frac{1}{4}\sum_{j,l=1}^{N(\omega_o)}\frac{\beta_l(\omega_o)}{\beta_j(\omega_o)}\phi_j^2(x_\star)\phi_l^2(x_\star)W_j^{(l)}(\omega_o,\beta_j'(\omega_o)Z,Z). \tag{5.23}$$

5.1.5. Statistical stability. Let us use (5.15) to bound the relative standard deviation

$$\frac{\sqrt{V(\vec{x}_\star)}}{|E\{\mathcal{I}(\vec{x}_\star)\}|} \geq C(\omega_o)\varepsilon^{1-\frac{\sigma}{2}} e^{\mathcal{D}_{\min}(\omega_o)Z}\mathcal{F}^{1/2}(\omega_o, Z, x_\star), \tag{5.24}$$

where $C(\omega_o)$ is an $O(1)$ coefficient that does not depend on Z. We show below that, for long enough ranges, $\mathcal{F} = O\left[1/(ZN(\omega_o))\right]$, so the bound in (5.24) becomes

$$\frac{\sqrt{V(\vec{x}_\star)}}{|E\{\mathcal{I}(\vec{x}_\star)\}|} \gtrsim O\left[\frac{\varepsilon^{1-\frac{\sigma}{2}} e^{\mathcal{D}_{\min}(\omega_o)Z}}{\sqrt{N(\omega_o)Z}}\right]. \tag{5.25}$$

This illustrates how the bandwidth $\varepsilon^\sigma B$, the number $N(\omega_o)$ of propagating modes, the central frequency ω_o, and the scaled range Z affect the stability of the imaging function. For a fixed central frequency and range, the stability improves in deeper waveguides that support more propagating modes, as well as for broad band pulses. However, the improvement is marginal since the relative standard deviation is likely to remain large due to the exponential factor $e^{\mathcal{D}_{\min}(\omega_o)Z}$. As we increase Z and ω_o (i.e., $\mathcal{D}_{\min}(\omega_o)$), the method becomes statistically unstable, as illustrated in Figures 3.3 and 3.6.

Long range estimation of $\mathcal{F}$. Let us recall from [11, section 20.6.2] that the matrix $\Gamma^{(c)}(\omega_o) = \left(\Gamma^{(c)}_{jl}(\omega_o)\right)$ in the right-hand side of (5.19) is negative semidefinite, with null space in the span of $(1, 1, \ldots, 1)^T$. Its largest eigenvalue, which is less than zero, is denoted by $-1/L_e$, where L_e is called the equipartition distance, because it quantifies the range scale over which the entries in the matrix exponential

$$U_{jl}(\omega_o, Z) = \left\{e^{\Gamma^{(c)}(\omega_o)Z}\right\}_{jl} = \lim_{\varepsilon\to 0} E\left\{T^\varepsilon_{jl}(\omega_o, Z)\overline{T^\varepsilon_{jl}}(\omega_o, Z)\right\} = \int d\tau\, \mathcal{W}^{(l)}_j(\omega, \tau, Z) \tag{5.26}$$

tend to the limit uniform[3] distribution

$$\sup_{j,l}\left|U_{jl}(\omega_o, Z) - \frac{1}{N(\omega_o)}\right| \leq O\left(e^{-Z/L_e}\right). \tag{5.27}$$

We are interested in the limit of $\mathcal{W}^{(l)}_j(\omega_o, \tau, Z)$, whose Fourier transform $\widehat{\mathcal{W}}^{(l)}_j(\omega_o, h, Z)$ satisfies

$$\widehat{\mathcal{W}}^{(l)}_j(\omega_o, h, Z) = \left\{\exp\left[\left(ih\mathcal{B}'(\omega_o) + \Gamma^{(c)}(\omega_o)\right)Z\right]\right\}_{jl} \tag{5.28}$$

for $\mathcal{B}'(\omega_o) = \mathrm{diag}\left(\beta'_1(\omega_o), \ldots, \beta'_{N(\omega_o)}(\omega_o)\right)$. It is estimated in [11, section 20.6.2], and the convergence is at the same rate as in (5.27). The continuum density tends to a Gaussian profile

$$W^{(l)}_j(\omega_o, \tau, Z) \approx \frac{1}{N(\omega_o)}\frac{1}{\sqrt{2\pi\sigma^2_e(\omega_o)Z}} e^{-\frac{(\tau-\beta'(\omega_o)Z)^2}{2\sigma^2_e(\omega_o)Z}}, \qquad Z \gg L_e, \tag{5.29}$$

[3]The long range limit of vector $(U_{1,l}, \ldots, U_{N,l})^T$ in (5.26) is in span$\{(1, 1, \ldots, 1)^T\}$, the null space of $\Gamma^{(c)}$, and the normalization constant $1/N$ comes from the fact that $T^\varepsilon(\omega_o, Z)$ is a unitary matrix, so the energy is conserved [11, section 20.2.6].

traveling at mean group velocity

$$\beta'(\omega_o) = \frac{1}{N(\omega_o)} \sum_{j=1}^{N(\omega_o)} \beta'_j(\omega_o) \tag{5.30}$$

and of variance $\sigma_e^2(\omega_o)Z$, estimated in [11, section 20.6.2] to be of the order

$$\sigma_e^2(\omega_o) \approx \frac{2L_e}{N(\omega_o)} \sum_{j=1}^{N(\omega_o)} \left[\beta'_j(\omega_o) - \beta'(\omega_o)\right]^2. \tag{5.31}$$

Thus,

$$\mathcal{F}(\omega_o, Z, x_\star) \approx \frac{\left[2\pi\sigma_e^2(\omega_o)\right]^{-1/2}}{4N(\omega_o)Z^{1/2}} \sum_{j,l=1}^{N(\omega_o)} \frac{\beta_l(\omega_o)}{\beta_j(\omega_o)} \phi_j^2(x_\star)\phi_l^2(x_\star) e^{-\frac{(\beta'_j(\omega_o)-\beta'(\omega_o))^2}{2\sigma_e^2(\omega_o)}Z},$$

with decoupled sums over j and l. Assuming a large $N = N(\omega_o)$, we get

$$\begin{aligned}\sum_{l=1}^{N} \beta_l(\omega_o)\phi_l^2(x_\star) &\approx \frac{8\pi}{\lambda_o^2 N} \sum_{l=1}^{N} \sqrt{1 - \frac{l^2}{N^2}} \sin^2\left(\frac{l}{N}\frac{2\pi x_\star}{\lambda_o}\right) \\ &\approx \frac{8\pi}{\lambda_o^2} \int_0^1 d\xi \sqrt{1-\xi^2} \sin^2\left(\xi \frac{2\pi x_\star}{\lambda_o}\right),\end{aligned}$$

which is $O(1)$. The sum over j is

$$\sum_{l=1}^{N} \frac{\phi_j^2(x_\star)}{\beta_j(\omega_o)} e^{-\frac{(\beta'_j(\omega_o)-\beta'(\omega_o))^2}{2\sigma_e^2(\omega_o)}Z} \approx \frac{2}{\pi} \int_0^1 d\xi \, \frac{\sin^2\left(\xi\frac{2\pi x_\star}{\lambda_o}\right)}{\sqrt{1-\xi^2}} e^{-\frac{Z}{2\sigma_e^2(\omega_o)}\left[\frac{1}{c_o}/\sqrt{1-\xi^2}-\beta'(\omega_o)\right]^2}, \tag{5.32}$$

and since $Z/\sigma_e^2(\omega_o) \sim Z/L_e \gg 1$, we have a Laplace-type integral [3, section 6.4] that can be estimated in the vicinity of ξ satisfying

$$\frac{1}{c_o}/\sqrt{1-\xi^2} = \beta'(\omega_o) = \frac{1}{N}\sum_{j=1}^{N} \frac{1}{c_o}/\sqrt{1-\frac{j^2}{N^2}} \approx \frac{\pi}{2c_o}.$$

We get that (5.32) is $O(Z^{-1/2})$, and thus $\mathcal{F} = O\left[1/(ZN(\omega_o))\right]$.

5.2. Matched field and CINT. The CINT function follows from (2.8):

$$\begin{aligned}\mathcal{I}^{CINT}(\vec{x}^s) = &\int \frac{d\omega}{2\pi} \int \frac{d\omega'}{2\pi} \widehat{\chi}_\Omega\left(\frac{\omega-\omega'}{\varepsilon^2}\right) \int_{\mathcal{A}} dr\, \widehat{p}(\omega, r, z_{\mathcal{A}}) \overline{\widehat{G}_o}(\omega, r, z_{\mathcal{A}}; \vec{x}^s) \\ &\times \int_{\mathcal{A}} dr'\, \overline{\widehat{p}}(\omega', r', z_{\mathcal{A}}) \widehat{G}_o(\omega', r', z_{\mathcal{A}}; \vec{x}^s).\end{aligned} \tag{5.33}$$

Since the decoherence frequency is $\Omega_d = \varepsilon^2\Omega$, it back propagates cross-correlations of the received traces over long time windows $\chi_\Omega(\varepsilon^2 t)$ of support $(\varepsilon^2\Omega)^{-1}$. The conventional (Bartlett) matched field function is

$$\mathcal{I}^{MF}(\vec{x}^s) = \int \frac{d\omega}{2\pi} \left| \int_{\mathcal{A}} dr\, \overline{\widehat{p}}(\omega, r, z_{\mathcal{A}}) \widehat{G}_o(\omega, r, z_{\mathcal{A}}; \vec{x}^s) \right|^2. \tag{5.34}$$

Now, let us compute the statistical mean of (5.33) and (5.34), in order to understand how CINT and matched field are expected to focus.

5.2.1. The statistical mean. Substituting (4.23) and (5.1) into (5.33)–(5.34), and setting $z_{\mathcal{A}} = Z/\varepsilon^2$ and $z_{\mathcal{A}} - z^s = Z^s/\varepsilon^2$, we get

$$E\left\{\mathcal{I}^{CINT}(\vec{x}^s)\right\} = \frac{1}{4}\sum_{j,l,j',l'=1}^{N(\omega_o)} \sqrt{\frac{\beta_l(\omega_o)\beta_{l'}(\omega_o)}{\beta_j(\omega_o)\beta_{j'}(\omega_o)}}\phi_l(x_\star)\phi_{l'}(x_\star)\phi_j(x^s)\phi_{j'}(x^s)$$
$$\times \int \frac{dh}{2\pi}\int \frac{dh'}{2\pi}\,\widehat{f}_B(h)\,\overline{\widehat{f}_B}(h')\widehat{\chi}_\Omega\left(\frac{h-h'}{\varepsilon^{2-\sigma}}\right) E\left\{T^\varepsilon_{jl}(\omega_o+\varepsilon^\sigma h, Z)\overline{T^\varepsilon_{j'l'}}(\omega_o+\varepsilon^\sigma h', Z)\right\}$$
$$\times\, e^{i\left[\beta_j(\omega_o+\varepsilon^\sigma h)-\beta_{j'}(\omega_o+\varepsilon^\sigma h')\right]\frac{(Z-Z^s)}{\varepsilon^2}} \tag{5.35}$$

for the CINT function and

$$E\left\{\mathcal{I}^{MF}(\vec{x}^s)\right\} = \frac{1}{4}\sum_{j,l,j',l'=1}^{N(\omega_o)} \sqrt{\frac{\beta_l(\omega_o)\beta_{l'}(\omega_o)}{\beta_j(\omega_o)\beta_{j'}(\omega_o)}}\phi_l(x_\star)\phi_{l'}(x_\star)\phi_j(x^s)\phi_{j'}(x^s)$$
$$\times \int \frac{dh}{2\pi}\left|\widehat{f}_B(h)\right|^2 E\left\{T^\varepsilon_{jl}(\omega_o+\varepsilon^\sigma h, Z)\overline{T^\varepsilon_{j'l'}}(\omega_o+\varepsilon^\sigma h, Z)\right\}$$
$$\times\, e^{i\left[\beta_j(\omega_o+\varepsilon^\sigma h)-\beta_{j'}(\omega_o+\varepsilon^\sigma h)\right]\frac{(Z-Z^s)}{\varepsilon^2}} \tag{5.36}$$

for matched field. This is in the best possible case of full aperture and for $\sigma \in (1,2)$. The results are worse for partial apertures, as illustrated in Figure 3.5.

To estimate (5.35), let us change variables:

$$\frac{h+h'}{2} \rightsquigarrow h, \qquad h - h' \rightsquigarrow \varepsilon^{2-\sigma}\widetilde{h}.$$

We obtain from Lemma 5.2 that

$$E\left\{\mathcal{I}^{CINT}(\vec{x}^s)\right\} \approx \frac{\varepsilon^{2-\sigma}\|f_B\|^2}{4}\sum_{j,l=1}^{N(\omega_o)}\frac{\beta_l(\omega_o)}{\beta_j(\omega_o)}\phi_l^2(x_\star)\phi_j^2(x^s)$$
$$\times \int d\tau W_j^{(l)}(\omega_o,\tau,Z)\,\chi_\Omega\left(\beta_j'(\omega_o)Z^s-\tau\right), \tag{5.37}$$

where we neglect the terms that decay exponentially in Z, and we let $\widehat{f}_B(h\pm\varepsilon^{2-\sigma}\widetilde{h}/2) \approx \widehat{f}_B(h)$. Now, recall that $\widehat{\chi}_\Omega(h)$ is supported in the frequency interval $[-\Omega,\Omega]$, which means that $\chi_\Omega(t)$ has time support $\sim 1/\Omega$. Assuming $\Omega \gg 1$, so that $\varepsilon^{2-\sigma}\Omega \ll B$, we get

$$E\left\{\mathcal{I}^{CINT}(\vec{x}^s)\right\} \approx \frac{\varepsilon^{2-\sigma}\|f_B\|^2}{4}\sum_{j,l=1}^{N(\omega_o)}\frac{\beta_l(\omega_o)}{\beta_j(\omega_o)}\phi_l^2(x_\star)\phi_j^2(x^s)W_j^{(l)}(\omega_o,\beta_j'(\omega_o)Z^s,Z). \tag{5.38}$$

Similarly, we estimate the expectation of the matched field function (5.36):

$$E\left\{\mathcal{I}^{MF}(\vec{x}^s)\right\} \approx \frac{\|f_B\|^2}{4}\sum_{j,l=1}^{N(\omega_o)}\frac{\beta_l(\omega_o)}{\beta_j(\omega_o)}\phi_l^2(x_\star)\phi_j^2(x^s)U_j^{(l)}(\omega_o,Z), \tag{5.39}$$

with $U_j^{(l)}(\omega_o,Z)$ given by (5.26).

5.3. Conclusions. Although the mean CINT and matched field functions do not decay exponentially in Z and/or ω_o, as was the case with $E\{\mathcal{I}(\vec{x}^s)\}$, they are not useful in localizing the source because they do not focus at $\vec{x}_\star$. The matched field function (5.39) does not have any range information, and it does not focus in the transverse direction. Indeed, recalling (5.27), we get that as Z/L_e grows,

$$E\left\{\mathcal{I}^{MF}(\vec{x}^s)\right\} \to \frac{\|f_B\|^2}{4N(\omega_o)} \sum_{l=1}^{N(\omega_o)} \beta_l(\omega_o)\phi_l^2(x_\star) \sum_{j=1}^{N(\omega_o)} \frac{\phi_j^2(x^s)}{\beta_l(\omega_o)}, \tag{5.40}$$

and there is no focusing in x^s. That is, the function does not exhibit a peak at $x^s \approx x^\star$. Returning to the results in Figure 3.4, we note that while $\mathcal{I}^{MF}(\vec{x}^s)$ localizes the source in case (i), where $Z \approx L_e$, it gives no range or cross-range information in case (iv), where $Z \approx 2.2L_e$. This is what our analysis predicts.

The CINT function does not focus any better in the transverse direction, but it has some range information through the evaluation of $W_j^{(l)}(\omega_o, \tau, Z)$ at $\tau = \beta_j'(\omega_o)Z^s$. However, due to the dispersion induced by the random medium, $W_j^{(l)}(\omega_o, \tau, Z)$ peaks far away from $\tau = \beta_j'(\omega_o)Z$. This means that each term in (5.38) peaks at a different Z^s, and the range support of $E\left\{\mathcal{I}^{CINT}(\vec{x}^s)\right\}$ is spread out, as in case (iv) in Figure 3.4. Explicitly, as Z/L_e grows, the peak of $W_j^{(l)}(\omega_o, \tau, Z)$ approaches $\tau = \beta'(\omega_o)Z$, and the j term in (5.38) gives a large contribution at range

$$Z^s(j) = \frac{\beta'(\omega_o)}{\beta_j'(\omega_o)} Z.$$

The range support of (5.38) is then between $Z^s(1)$ and $Z^s(N(\omega_o))$, which is a large interval.

To calculate the variance of $\mathcal{I}^{CINT}$ and $\mathcal{I}^{MF}$, we need the fourth order multifrequency moments of $T_{jl}^\varepsilon(\omega, Z)$, which are given in the next section and in Appendix C. However, since we have already shown that the mean CINT and matched field functions do not focus at the source, there is no point in analyzing their statistical stability.

6. Incoherent source localization. We introduce in this section an incoherent source localization method. As we have learned from the analysis in section 5, the mean field $E\{\widehat{p}(\omega, r, z_{\mathcal{A}})\}$ decays exponentially in $Z = \varepsilon^2 z_{\mathcal{A}}$, signaling the rapid loss of coherence of the pressure field recorded at the array. We have also seen that expectations of cross-correlations of the traces persist at long ranges, and this is why we use them to obtain a statistically stable source localization. Matched field and CINT work with cross-correlations as well, but they do not focus because the cross-correlations back propagated with the Green's function $\widehat{G}_o$ do not add coherently. We estimate instead the source location by minimizing a certain misfit function.

If we took frequency correlations into account, like in CINT, we would work with

$$\begin{aligned}\mathcal{F}(\omega_o, t, r, r') &= \int_{|\omega-\omega_o|\le\varepsilon^\sigma B} \frac{d\omega}{2\pi}\,\varepsilon^2 \int \frac{dh}{2\pi}\,\widehat{p}(\omega, r, z_{\mathcal{A}})\overline{\widehat{p}}(\omega - \varepsilon^2 h, r', z_{\mathcal{A}})e^{-iht} \\ &\approx \int_{|\omega-\omega_o|\le\varepsilon^\sigma B} \frac{d\omega}{2\pi}\,\varepsilon^2 \int \frac{dh}{2\pi}\,e^{-iht}\,E\left\{\widehat{p}(\omega, r, z_{\mathcal{A}})\overline{\widehat{p}}(\omega - \varepsilon^2 h, r', z_{\mathcal{A}})\right\}\end{aligned} \tag{6.1}$$

for receiver transverse coordinates $r, r' \in \mathcal{A}$ and for broad band pulses with $\sigma < 2$. Otherwise, we would work with the cross-correlations

$$\varepsilon^{-2}\int dt\,\mathcal{F}(\omega_o,t,r,r') = \int_{|\omega-\omega_o|\le\varepsilon^\sigma B}\frac{d\omega}{2\pi}\,\widehat{p}(\omega,r,z_{\mathcal{A}})\overline{\widehat{p}}(\omega,r',z_{\mathcal{A}})$$

$$\approx \int_{|\omega-\omega_o|\le\varepsilon^\sigma B}\frac{d\omega}{2\pi}\,E\left\{\widehat{p}(\omega,r,z_{\mathcal{A}})\overline{\widehat{p}}(\omega,r',z_{\mathcal{A}})\right\}, \tag{6.2}$$

like in matched field. The integrands in (6.1) and (6.2) decorrelate over ω offsets that exceed $O(\varepsilon^2)$ [11, section 20.6], and this is why we can approximate the integrals over the broad band by their statistical expectation. We give more details in section 6.1.2, where we also show that the self-averaging does not hold for narrow band pulses with bandwidth $\varepsilon^2 B$.

Now, let us use Lemma 5.2 to compute the expectations in (6.1) and (6.2). We obtain after calculations that are similar to those in section 5.2.1 that

$$\mathcal{F}(\omega_o,t,r,r') \approx \frac{\varepsilon^{2-\sigma}\|f_B\|^2}{4}\sum_{j,l=1}^{N(\omega_o)}\frac{\beta_l(\omega_o)}{\beta_j(\omega_o)}\phi_l^2(x_\star)\phi_j(r)\phi_j(r')\mathcal{W}_j^{(l)}(\omega_o,t,Z) \tag{6.3}$$

and

$$\int dt\,\mathcal{F}(\omega_o,t,r,r') \approx \frac{\varepsilon^{2-\sigma}\|f_B\|^2}{4}\sum_{j,l=1}^{N(\omega_o)}\frac{\beta_l(\omega_o)}{\beta_j(\omega_o)}\phi_l^2(x_\star)\phi_j(r)\phi_j(r')\int dt\,\mathcal{W}_j^{(l)}(\omega_o,t,Z). \tag{6.4}$$

The approximation assumes a long enough range to neglect the exponentially decaying terms in the second moments in Lemma 5.2 and a bandwidth $\varepsilon^\sigma B$ with $\sigma\in(1,2)$.

Equations (6.3) and (6.4) show how the cross-correlations of the data traces carry information about the source location. The cross-range $x_\star$ appears the same way in (6.3) and (6.4) in the argument of ϕ_l^2. The scaled range Z is in the Wigner transform. Because the time integral of the Wigner transform approaches $1/N(\omega_o)$ as the range grows, as shown in (5.27), the cross-correlations (6.2) are not useful for determining the source range. The range Z determines the time peak location of $\mathcal{W}_j^{(l)}(\omega_o,t,Z)$, and this is why we can estimate it from the cross-correlations (6.1).

The source localization described below is in two steps: First, we show in section 6.1 how to determine the range Z and the correlation function of the random fluctuations of the wave speed using the cross-correlations (6.3). Then, we show in section 6.2 how to estimate the source cross-range $x_\star$. Because the use of frequency correlations does not give additional information about $x_\star$, we estimate the cross-range with the simpler function (6.4). We study with theory and numerical simulations the estimation functions and show that the cross-range localization requires that Z be at most $\sim L_e$. The range estimation can be carried out for much larger distances of propagation. We also study the statistical stability of the estimation, which requires fourth order multifrequency moments of the transfer matrix, computed in Appendix C in the limit $\varepsilon\to 0$.

6.1. Range estimation. The information about the scaled range Z is encoded in the cross-correlations $\mathcal{F}(\omega_o,t,r,r')$ in a complicated way via the Wigner transform $\mathcal{W}_j^{(l)}(\omega_o,t,Z)$. To untangle it, we use the receiver coordinates and project $\mathcal{F}(\omega_o,t,r,r')$ onto the waveguide modes

$$\int_{\mathcal{A}} dr\,\phi_j(r)\int_{\mathcal{A}} dr'\,\phi_j(r')\,\mathcal{F}(\omega_o,t,r,r')$$

$$= \int_{|\omega-\omega_o|\le\varepsilon^\sigma B}\frac{d\omega}{2\pi}\,\varepsilon^2\int\frac{dh}{2\pi}\widehat{P}_j(\omega,z_{\mathcal{A}})\overline{\widehat{P}_j}(\omega-\varepsilon^2 h,z_{\mathcal{A}})e^{-iht}, \tag{6.5}$$

where

$$\widehat{P}_j(\omega, z_{\mathcal{A}}) = \int_{\mathcal{A}} dr\, \widehat{p}(\omega, r, z_{\mathcal{A}})\phi_j(r). \tag{6.6}$$

Recalling the theoretical model (6.3), and assuming for a moment the ideal case of a full aperture $\mathcal{A} = [0, X]$, we obtain by the orthogonality of the eigenfunctions that

(6.7)

$$\int_{\mathcal{A}} dr\, \phi_j(r) \int_{\mathcal{A}} dr'\, \phi_j(r')\, \mathcal{F}(\omega_o, t, r, r') \approx \frac{\varepsilon^{2-\sigma}\|f_B\|^2}{4} \sum_{l=1}^{N(\omega_o)} \frac{\beta_l(\omega_o)}{\beta_j(\omega_o)} \phi_l^2(x_\star) \mathcal{W}_j^{(l)}(\omega_o, t, Z).$$

The range Z could be determined from (6.7) if we knew the transport speed. In weak random media, the transport speed is close to $\beta_j'(\omega_o)$, and Z can be estimated from the maxima over the search ranges Z^s of the migrated projected cross-correlations (6.7) with travel times $\beta_j'(\omega_o)Z^s$. We are interested in strong random media, where the transport speed is different from $\beta_j'(\omega_o)$ and must be estimated as we search for range Z.

Our estimation is based on the "dispersion function"

$$\mathcal{R}(\zeta, j) = \int_{\mathcal{A}} dr\, \phi_j(r) \int_{\mathcal{A}} dr'\, \phi_j(r')\, \mathcal{F}(\omega_o, t = \beta_j'(\omega_o)\zeta, r, r'), \tag{6.8}$$

where ζ is the scaled range at which we migrate approximately the cross-correlations with the incorrect speed $\beta_j'(\omega_o)$. Therefore, $\mathcal{R}(\zeta, j)$ peaks at $\zeta = \zeta_j$, which in general is not equal to Z. The algorithm described below estimates Z by comparing the dispersion function $\mathcal{R}(\zeta, j)$ with its theoretical model $\mathcal{R}^M(\zeta, j; Z^s)$ for a hypothetical source at search range Z^s. More specifically, it approximates Z by the minimizer over all Z^s of an objective function that measures the misfit between $\mathcal{R}(\zeta, j)$ and $\mathcal{R}^M(\zeta, j; Z^s)$. The transport speed is computed using the transport equations stated in Lemma 5.2, assuming a known correlation function $\mathcal{C}$ of the fluctuations of the wave speed. In fact, we solve these equations to compute the Wigner transform that enters the theoretical model $\mathcal{R}^M(\zeta, j; Z^s)$. If the correlation function $\mathcal{C}$ is not known, it can be estimated from the misfit between $\mathcal{R}(\zeta, j)$ and $\mathcal{R}^M(\zeta, j; Z^s)$ as well.

To state the algorithm, we need the following proposition proved in Appendix B. It applies to broad and narrow band pulses, and to partial apertures, where there is additional mode coupling due to the integrals

$$\mathcal{M}_{jq} = \int_{\mathcal{A}} dr\, \phi_j(r)\phi_q(r).$$

PROPOSITION 6.1. *The theoretical expected model of* (6.8) *is given by*

$$E\{\mathcal{R}(\zeta, j)\} \approx \frac{\varepsilon^{2-\sigma}\|f_B\|^2}{4} \sum_{q,l=1}^{N(\omega_o)} \mathcal{M}_{jq}^2 \frac{\beta_l(\omega_o)}{\beta_q(\omega_o)} \phi_l^2(x_\star) \mathcal{W}_q^{(l)}(\omega_o, \beta_j'(\omega_o)\zeta, Z) \tag{6.9}$$

in the broad band case $\sigma \in (1, 2)$. In narrow band $\sigma = 2$, we have at long ranges

$$\begin{aligned} E\{\mathcal{R}(\zeta, j)\} \approx \frac{1}{4} \sum_{q,l=1}^{N(\omega_o)} \mathcal{M}_{jq}^2 \frac{\beta_l(\omega_o)}{\beta_q(\omega_o)} \phi_l^2(x_\star) \int d\tau \mathcal{W}_q^{(l)}(\omega_o, \beta_j'(\omega_o)\zeta - \tau, Z) \\ \times \int d\widetilde{t}\, \frac{B}{\pi} \operatorname{sinc}\left(B\widetilde{t}\right) f_B\left(\tau + \frac{\widetilde{t}}{2}\right) \overline{f_B}\left(\tau - \frac{\widetilde{t}}{2}\right). \end{aligned} \tag{6.10}$$

6.1.1. The estimation algorithm. We now introduce an algorithm that estimates the scaled range source Z based on the dispersive effect induced by the random medium.

ALGORITHM 6.2. *This algorithm assumes a known correlation function of the random fluctuations, so that we can compute the matrix* $\Gamma^{(c)}(\omega_o)$. *It also assumes a fixed bandwidth* $\omega \in [\omega_o - \varepsilon^\sigma B, \omega_o + \varepsilon^\sigma B]$ *of the pulse* $f^\varepsilon(t)$. *The estimation involves three steps.*

Step 1. *Given the array data, compute* $\mathcal{R}(\zeta, j)$ *using* (6.8) *for modes* $j = 1, 2, \ldots, N(\omega_o)$ *and* ζ *in a search interval that includes its peaks* ζ_j.

Step 2. *Determine the set* $\mathcal{S}$ *of modes for which*

$$|\mathcal{R}(\zeta_j, j)| = \max_\zeta |\mathcal{R}(\zeta, j)| > \delta, \tag{6.11}$$

with δ *a user-defined tolerance.*

Step 3. *Estimate* Z *by* $Z^\star$, *the minimizer of the objective function*

$$\mathbb{O}(Z^s) = \sum_{j\in\mathcal{S}} \int d\zeta \left| \frac{\mathcal{R}(\zeta, j)}{\mathcal{R}(\zeta_j, j)} - \frac{\mathcal{R}^M(\zeta, j; Z^s)}{\mathcal{R}^M(\zeta_j^M, j; Z^s)} \right|^2, \tag{6.12}$$

where $\mathcal{R}^M(\zeta, j; Z^s)$ *is the model of the expectation of* (6.8) *for a hypothetical source at range* $z^s = z_{\mathcal{A}} - Z^s/\varepsilon^2$ *from the array, and* ζ_j^M *is its peak. The integral in* (6.12) *extends over the search domain.*

Proposition 6.1 shows that in theory all the range information is in $\mathcal{W}_q^{(l)}$, which we approximate by taking the inverse Fourier transform of the matrix exponential (5.28). Since we do not know the source cross-range, we cannot define $\mathcal{R}^M$ by (6.9) or (6.10). Instead, we replace in these formulas $\phi_l^2(x_\star)$ by the constant $2/X$ and get

$$\mathcal{R}^M(\zeta, j; Z^s) = \frac{\varepsilon^{2-\sigma}\|f_B\|^2}{2X} \sum_{q,l=1}^{N(\omega_o)} \mathcal{M}_{jq}^2 \frac{\beta_l(\omega_o)}{\beta_q(\omega_o)} \mathcal{W}_q^{(l)}(\omega_o, \beta_j'(\omega_o)\zeta, Z^s) \tag{6.13}$$

in broad band and

$$\begin{aligned} \mathcal{R}^M(\zeta, j; Z^s) = \frac{1}{2X} \sum_{q,l=1}^{N(\omega_o)} \mathcal{M}_{jq}^2 \frac{\beta_l(\omega_o)}{\beta_q(\omega_o)} \int d\tau \mathcal{W}_q^{(l)}(\omega_o, \beta_j'(\omega_o)\zeta - \tau, Z^s) \\ \times \int d\widetilde{t}\, \frac{B}{\pi} \operatorname{sinc}\left(B\widetilde{t}\right) f_B\left(\tau + \frac{\widetilde{t}}{2}\right) \overline{f_B}\left(\tau - \frac{\widetilde{t}}{2}\right) \end{aligned} \tag{6.14}$$

in narrow band. This should have minimal effect on the range estimation, which is based on the variation of $\mathcal{R}(\zeta, j)$ in ζ. The cross-range $x_\star$ affects the actual peak value $\mathcal{R}(\zeta_j, j)$, which is why we normalize $\mathcal{R}$ in the objective function. We also filter out the modes for which $|\mathcal{R}(\zeta_j, j)|$ is below the threshold δ.

Algorithm 6.2 assumes that we know the correlation function

$$\mathcal{C}(x, x', z - z') = E\left\{\nu(x, z)\nu(x', z')\right\}$$

of the fluctuations. When we do not know $\mathcal{C}$, but have a priori information about how to model it, we can estimate it together with the source range.

ALGORITHM 6.3. *This algorithm is based on the a priori model*

$$\mathcal{C}^M(x - x', z - z'; \alpha^s, \ell^s) = \alpha^s \Theta\left[(x - x', z - z')/\ell^s\right] \tag{6.15}$$

of $\mathcal{C}$, where Θ is a given function of $O(1)$ support. It is parametrized by the search amplitude α^s and the search correlation length ℓ^s.

Steps 1 *and* 2 *are identical to those in Algorithm* 6.2.

Step 3. *Estimate $Z = Z^\star$ and the correlation function $\mathcal{C} \approx \mathcal{C}^M(x - x', z - z'; \alpha^\star, \ell^\star)$, where $(Z^\star, \alpha^\star, \ell^\star)$ is the minimizer of*

$$\mathbb{O}(Z^s, \alpha^s, \ell^s) = \sum_{j \in \mathcal{S}} \int d\zeta \left| \frac{\mathcal{R}(\zeta, j)}{\mathcal{R}(\zeta_j, j)} - \frac{\mathcal{R}^M(\zeta, j; Z^s, \alpha^s, \ell^s)}{\mathcal{R}^M(\zeta_j^M, j; Z^s, \alpha^s, \ell^s)} \right|^2 . \tag{6.16}$$

Here $\mathcal{R}^M(\zeta, j; Z^s, \alpha^s, \ell^s)$ is the model of the expectation of (6.8) *for a hypothetical source at range $z^s = z_{\mathcal{A}} - Z^s/\varepsilon^2$ and for fluctuations with correlation function* (6.15).

The essential assumption in this algorithm is the model of the correlation function of the fluctuations $\nu(\vec{x})$, which are supposed in (6.15) isotropic and stationary in range and cross-range. In principle, the algorithm could handle fluctuations that are anisotropic and not stationary in cross-range, so that $\mathcal{C}^M$ depends on more than two parameters. We do not have such results. In any case, it is expected that the more parameters there are in the model, the more difficult the estimation.

An essential question that arises is how sensitive the estimation is to the accuracy of the model (6.15). Our numerical experiments suggest that the range estimation is not too sensitive to the model $\mathcal{C}^M$. For example, in a simulation with $\varepsilon = 3\%$, central frequency 2.39kHz, and bandwidth 0.375kHz, Algorithm 6.3 returned essentially the same source range $Z^\star \approx Z$ for three models of $\mathcal{C}^M$. The first is Gaussian,

$$\mathcal{C}^M(x - x', z - z'; \alpha^s, \ell^s) = \alpha^s e^{-\frac{|\vec{x} - \vec{x}'|^2}{2(\ell^s)^2}}, \tag{6.17}$$

like the one used in the simulations of the array data. The second model is exponential,

$$\mathcal{C}^M(x - x', z - z'; \alpha^s, \ell^s) = \alpha^s e^{-\frac{|\vec{x} - \vec{x}'|}{\ell^s}}, \tag{6.18}$$

and the third is

$$\mathcal{C}^M(x - x', z - z'; \alpha^s, \ell^s) = \alpha^s \left(1 + \frac{|\vec{x} - \vec{x}'|}{\ell s}\right) e^{-\frac{|\vec{x} - \vec{x}'|}{\ell^s}}. \tag{6.19}$$

We note that, at high spatial frequencies, the Fourier transform (power spectral density) of (6.19) has power law behavior typical of multiscale random media.

With the Gaussian model we obtained

$$\alpha^\star \approx (2\pi\ell^2)^{-1} = 2.55\text{m}^{-2} \quad \text{and} \quad \ell^\star \approx \ell = 0.25\text{m},$$

as expected from (3.2). Naturally, the algorithm returned different parameters $\alpha^\star$ and $\ell^\star$ with the second and third models, but they all satisfied the normalization relation

$$\int d\vec{x}\, \mathcal{C}^M(\vec{x}) \approx \int d\vec{x}\, \mathcal{C}(\vec{x}) = 1.$$

This is not surprising, as it is not the correlation function per se that appears in the transport equations, but integrals of it multiplied by the waveguide modes and slowly oscillating cosine functions, as seen from Lemmas 5.1 and 5.2.

6.1.2. Statistical stability. To estimate the variance of the range estimation function (6.8), we need the fourth order moments of $T^\varepsilon(\omega, Z)$ at nearby frequencies. The transfer matrix decorrelates at frequency offsets that exceed $O(\varepsilon^2)$ [11], so we need to consider only $O(\varepsilon^2)$ frequency shifts. We derive all these moments in Appendix C, but we use only those for a subset of indexes relevant to the variance calculation at full aperture. The variance at partial aperture follows similarly, and we do not include it here to simplify the exposition.

The model of the estimation function (6.8) at full aperture is

$$\begin{aligned}\mathcal{R}(\zeta, j) \approx \frac{\varepsilon^{2-\sigma}}{4} \int_{-B}^{B} \frac{dh}{2\pi} \int_{-\Omega}^{\Omega} \frac{d\tilde{\omega}}{2\pi} \widehat{f}_B \left(h + \frac{\varepsilon^{2-\sigma}\tilde{\omega}}{2}\right) \overline{\widehat{f}_B} \left(h - \frac{\varepsilon^{2-\sigma}\tilde{\omega}}{2}\right) \\ \times \sum_{l,l'=1}^{N(\omega_o)} \sqrt{\frac{\beta_l(\omega_o)\beta_{l'}(\omega_o)}{\beta_j(\omega_o)\beta_{j'}(\omega_o)}} \phi_l(x_\star)\phi_{l'}(x_\star) T^\varepsilon_{jl} \left(\omega + \varepsilon^\sigma h + \frac{\varepsilon^2}{2}\tilde{\omega}, Z\right) \\ \times \overline{T^\varepsilon_{jl'}} \left(\omega_o + \varepsilon^\sigma h - \frac{\varepsilon^2}{2}\tilde{\omega}, Z\right) e^{i\tilde{\omega}(Z-\zeta)\beta'_j(\omega_o)}, \end{aligned} \tag{6.20}$$

and its variance

$$V(\zeta, j) = E\left\{|\mathcal{R}(\zeta, j)|^2\right\} - |E\{\mathcal{R}(\zeta, j)\}|^2$$

is estimated in the following proposition, proved in Appendix D.

PROPOSITION 6.4. *The variance $V(\zeta, j)$ of the estimation function at full aperture satisfies*

$$\frac{V(\zeta, j)}{|E\{\mathcal{R}(\zeta_j, j)\}|} \sim \frac{\varepsilon^2\Omega}{\varepsilon^\sigma B}, \tag{6.21}$$

where ζ_j is the peak of $|E\{\mathcal{R}(\zeta, j)\}|$. Since $\varepsilon^2\Omega$ is the decoherence frequency of $T^\varepsilon(\omega, Z)$ and $\varepsilon^\sigma B$ is the bandwidth of the pulse $\widehat{f}^\varepsilon$, this implies that the estimation function is statistically stable in the vicinity of its peak in broad band, where $\varepsilon^\sigma B \gg \varepsilon^2\Omega$. The function is not stable in narrow band regimes.

The proposition says that even though it may appear from the mean field model computed in Proposition 6.1 that we can estimate the range in narrow band, the estimation will not be reliable because the range estimation function $\mathcal{R}(\zeta, j)$ changes unpredictably with the realization of the random medium. We need a broad band regime in order to obtain statistically stable results. This conclusion is validated by extensive numerical simulations.

6.1.3. Numerical results. We present here numerical range estimation results in the setup described in section 3. The unknown source is at location $\vec{x}_\star = (5\lambda_c, 0)$ at unscaled range $z_{\mathcal{A}} = 494\lambda_c$ from the array.

We begin in Figure 6.1 with results at full aperture, $\varepsilon = 3\%$, central frequency 2.09kHz, and bandwidth 0.375kHz. This is the case considered in plot (iv) of Figure 3.4, where matched field and CINT do not work. We show in the top left plot in Figure 6.1 how the amplitude of $\mathcal{R}(\zeta_j, j)$ varies with j and indicate the threshold value $\delta = 0.2$ used in our estimation. The set $\mathcal{S}$ contains the mode indexes j with peak amplitudes above this threshold. The middle picture in the top row is a plot of $\mathcal{R}(\zeta, j)/\mathcal{R}(\zeta_j, j)$ for $j \in \mathcal{S}$. This is computed from the array data and enters the objective function at Step 3 of Algorithm 6.2. The abscissa in the plot is ζ/ε^2 in units of λ_c. The ordinate is the mode index in $\mathcal{S}$. Note how the dispersion effects induced

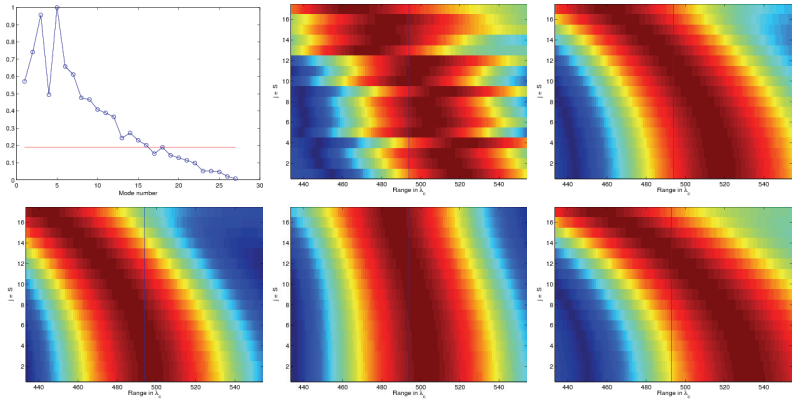

FIG. 6.1. *Range estimation results for $\varepsilon = 3\%$, central frequency 2.09kHz, and bandwidth 0.375kHz.* Top row: *Left: $\mathcal{R}(\zeta_j, j)$ and the threshold $\delta = 0.2$ for determining the set $\mathcal{S}$ of indexes. Middle: $\mathcal{R}(\zeta, j)$. Right: $\mathcal{R}^M(\zeta, j; Z^\star, \alpha^\star, \ell^\star)$.* Bottom row: $\mathcal{R}^M(\zeta, j; Z^s, \alpha^s, \ell^s)$ *for optimal Z^s, α^s, ℓ^s, unless specified otherwise. Left: $Z^s = Z^\star - 20\varepsilon^2\lambda_c$. Middle: $\ell^s = \ell^s/2$. Right: $\alpha^s = 1.34\alpha^\star$.*

by the random medium cause $\mathcal{R}(\zeta, j)$ to peak at ranges different from the true one, indicated by the vertical black line.

$\mathcal{R}^M(\zeta, j; Z^\star, \alpha^\star, \ell^\star)/\mathcal{R}^M(\zeta_j^M, j; Z^\star, \alpha^\star, \ell^\star)$ for $j \in \mathcal{S}$ and the optimal parameters returned by the algorithm is shown in the right picture in the top row of Figure 6.1. The optimization is done with the MATLAB function *fmincon*. Compare this picture with the ones in the bottom row, where we fix two parameters at the optimal values but vary the third one. In the left picture, we set $Z^s - Z^\star = 20\varepsilon^2\lambda_c$ and note the resulting range shift. In the middle picture, we set $\ell^s = \ell^\star/2$ and see a different dispersive behavior (the peaks have a different distribution around the true range value). The right picture is for $\alpha^s = 1.34\alpha^\star$ and again shows a different dispersive behavior.

In Figure 6.2 we show cross-sections of the objective function $\mathbb{O}(Z^s, \alpha^s, \ell^s)$ for two realizations of the random medium and at full aperture. The top row is for $\varepsilon = 2\%$, at central frequency 2.69kHz and bandwidth 0.375kHz, which is the case in plot (i) of Figure 3.4, where both matched field and CINT work. The bottom row is for $\varepsilon = 3\%$, at central frequency 2.09kHz and bandwidth 0.375kHz, which is the same as in plot (iv) of Figure 3.4, where matched field and CINT do not work. Figure 6.2 illustrates that the objective function has a clear minimum around the true value of the parameter indicated by a circle. The figure also shows that the results are essentially the same in the two realizations of the medium, as stated in Proposition 6.4.

Figure 6.3 shows cross-sections of the objective function $\mathbb{O}(Z^s, \alpha^s, \ell^s)$ at partial aperture. Here $\varepsilon = 2\%$, the central frequency is 2.69kHz, and the bandwidth is 0.45kHz. The top row is for 40% aperture $\mathcal{A} = [0, 8\lambda_c]$, and the bottom row is for 20% aperture $\mathcal{A} = [0, 4\lambda_c]$. The analogous plots for the medium with $\varepsilon = 3\%$ and central frequency 2.09kHz are in Figure 6.4. The results are almost the same as in Figure 6.2, except for the bottom left picture, where the estimated α^s is slightly off.

6.2. Cross-range estimation. Since the cross-range information appears the same way in the cross-correlations of the array data traces, whether we exploit frequency correlation or not, we base the estimation on the simpler model (6.4). Specifically, we work with $\int dt\mathcal{F}(\omega_o, t, r, r')$ and use the receiver coordinates to define the

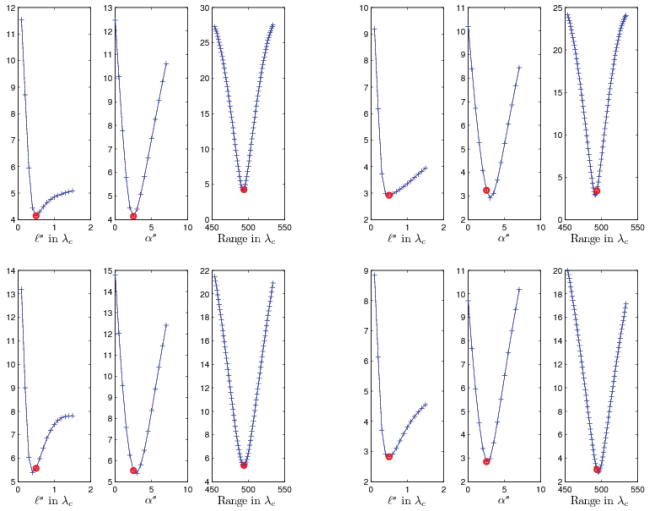

FIG. 6.2. *Cross-sections of the range estimation objective function* $\mathbb{O}(Z^s, \alpha^s, \ell^s)$. *In each plot we fix two parameters at the optimal values and display the variation in the third parameter. The true value of the parameters is indicated by a circle. The results are at full aperture.* Top row: *two realizations at* $\varepsilon = 2\%$, *central frequency* $2.69kHz$, *and bandwidth* $0.375kHz$. Bottom row: *two realizations at* $\varepsilon = 3\%$, *central frequency* $2.09kHz$, *and bandwidth* $0.375kHz$.

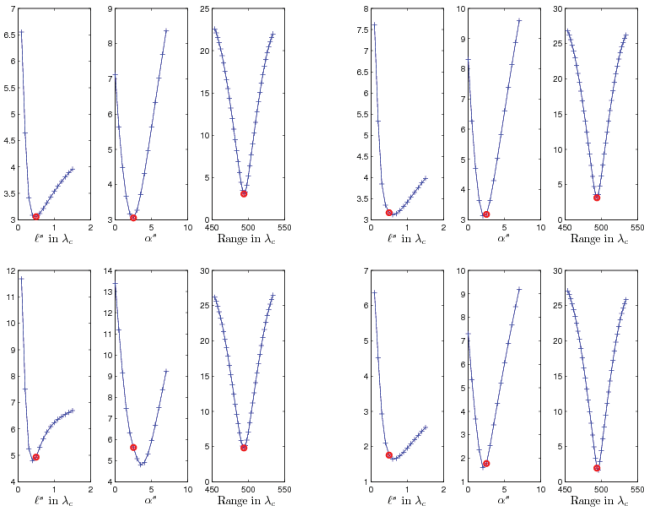

FIG. 6.3. *Cross-sections of the range estimation objective function* $\mathbb{O}(Z^s, \alpha^s, \ell^s)$. *The results are at partial aperture at* $\varepsilon = 2\%$, *central frequency* $2.69kHz$, *and bandwidth* $0.45kHz$. Top row: *two realizations at* $\mathcal{A} = [0, 8\lambda_c]$. Bottom row: *two realizations at* $\mathcal{A} = [0, 4\lambda_c]$.

cross-range estimation function

$$\begin{aligned}\mathcal{X}(j) &= \int dt \int_{\mathcal{A}} dr\, \phi_j(r) \int_{\mathcal{A}} dr'\, \phi_j(r') \mathcal{F}(\omega_o, t, r, r') \\ &= \varepsilon^2 \int_{|\omega-\omega_o|\le \varepsilon^\sigma B} \frac{d\omega}{2\pi} \widehat{P}_j(\omega, z_{\mathcal{A}}) \overline{\widehat{P}_j}(\omega, z_{\mathcal{A}}),\end{aligned} \tag{6.22}$$

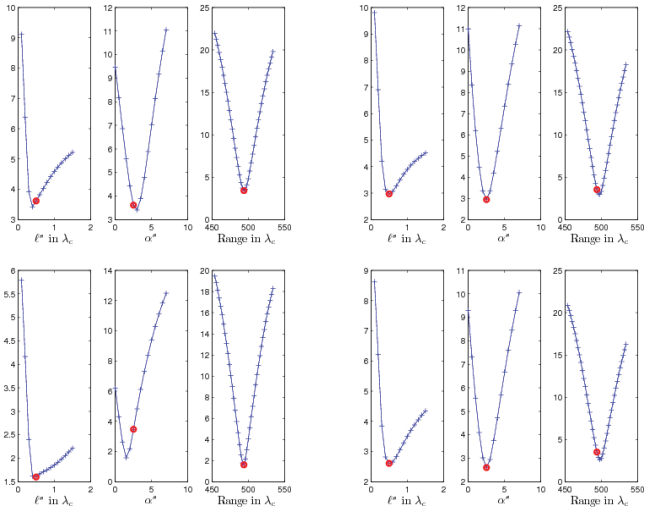

FIG. 6.4. *Cross-sections of the range estimation objective function* $\mathbb{O}(Z^s, \alpha^s, \ell^s)$. *The results are at partial aperture at* $\varepsilon = 3\%$, *central frequency* $2.69kHz$, *and bandwidth* $0.45kHz$. Top row: *two realizations at* $\mathcal{A} = [0, 8\lambda_c]$. Bottom row: *two realizations at* $\mathcal{A} = [0, 4\lambda_c]$.

with $\widehat{P}_j$ defined by (6.6). The estimate of $x_\star$ is the minimizer over x^s of an objective function that measures the misfit between $\mathcal{X}(j)$ and its model $\mathcal{X}^M(j; x^s)$ for a hypothetical source at $\vec{x}^s = (x^s, Z^\star)$. Here $Z^\star$ is the range estimate obtained as explained in the previous section.

The model is

$$\mathcal{X}^M(j; x^s) = \frac{\varepsilon^{2-\sigma}}{4} \sum_{q,l,q',l'=1}^{N(\omega_o)} \mathcal{M}_{jq}\mathcal{M}_{jq'} \sqrt{\frac{\beta_l(\omega_o)\beta'_l(\omega_o)}{\beta_q(\omega_o)\beta_{q'}(\omega_o)}}\phi_l(x^s)\phi_{l'}(x^s) \int_{-B}^{B} \frac{dh}{2\pi} |\widehat{f}_B(h)|^2$$

$$\times e^{i\frac{Z^\star}{\varepsilon^2}\left[\beta_q(\omega_o+\varepsilon^\sigma h)-\beta_{q'}(\omega_o+\varepsilon^\sigma h)\right]} E\left\{T^\varepsilon_{ql}(\omega_o+\varepsilon^\sigma h, Z^\star)\overline{T^\varepsilon_{q'l'}}(\omega_o+\varepsilon^\sigma h, Z^\star)\right\}, \tag{6.23}$$

where, by Lemma 5.2,

$$E\left\{T^\varepsilon_{ql}(\omega, Z^\star)\overline{T^\varepsilon_{q'l'}}(\omega, Z^\star)\right\} \approx (1-\delta_{qq'})\delta_{ql}\delta_{q'l'} e^{-\left[\mathcal{D}_q(\omega)+\mathcal{D}_{q'}(\omega)-\Gamma^{(1)}_{qq'}(\omega)\right]Z^\star + i\left[\mathcal{O}_q(\omega)-\mathcal{O}_{q'}(\omega)\right]Z^\star}$$
$$+ \delta_{qq'}\delta_{ll'}U_{ql}(\omega, Z^\star),$$

with $U_{ql}(\omega, Z^\star) = \int dt\, \mathcal{W}^{(l)}_q(\omega, t, Z^\star)$ given by (5.26). Equation (6.23) becomes

$$\mathcal{X}^M(j; x^s) \approx \frac{\varepsilon^{2-\sigma}}{4} \int_{-B}^{B} \frac{dh}{2\pi} |\widehat{f}_B(h)|^2$$
$$\times \left\{ \sum_{q,q'=1}^{N(\omega_o)} (1-\delta_{qq'})\mathcal{M}_{jq}\mathcal{M}_{jq'}\phi_q(x^s)\phi_{q'}(x^s) e^{i\frac{Z^\star}{\varepsilon^2}\left[\beta_q(\omega_o+\varepsilon^\sigma h)-\beta_{q'}(\omega_o+\varepsilon^\sigma h)\right]} \right.$$
$$\times e^{-\left[\mathcal{D}_q(\omega_o)+\mathcal{D}_{q'}(\omega_o)-\Gamma^{(1)}_{qq'}(\omega_o)\right]Z^\star + i\left[\mathcal{O}_q(\omega_o)-\mathcal{O}_{q'}(\omega_o)\right]Z^\star}$$
$$\left. + \sum_{q,l=1}^{N(\omega_o)} \mathcal{M}^2_{jq} \frac{\beta_l(\omega_o)}{\beta_q(\omega_o)} \phi^2_l(x^s) U_{ql}(\omega_o, Z^\star) \right\}, \tag{6.24}$$

and it simplifies to

$$\mathcal{X}^M(j;x^s) \approx \frac{\varepsilon^{2-\sigma}\|f_B\|^2}{4}\sum_{l=1}^{N(\omega_o)}\frac{\beta_l(\omega_o)}{\beta_j(\omega_o)}\phi_l^2(x^s)U_{jl}(\omega_o,Z^\star) \tag{6.25}$$

in the case of full aperture and for broad band pulses. Although it may appear that the broad band does not play a role in (6.25), we need it to get statistical stability. The variance calculation for $\mathcal{X}(j)$ is essentially the same as that for $\mathcal{R}(Z^s,j)$, and we do not repeat it here.

6.2.1. The estimation algorithm.

ALGORITHM 6.5. *The cross-range estimation is based on the minimization of the objective function*

$$\mathbb{O}(x^s) = \sum_{j\in\mathcal{S}}\left|\frac{\mathcal{X}(j)}{\langle\mathcal{X}(\cdot)\rangle} - \frac{\mathcal{X}^M(j;x^s)}{\langle\mathcal{X}^M(\cdot;x^s)\rangle}\right|^2, \tag{6.26}$$

where

$$\langle\mathcal{X}(\cdot)\rangle = \frac{1}{|\mathcal{S}|}\sum_{j\in\mathcal{S}}\mathcal{X}(j), \qquad \langle\mathcal{X}^M(\cdot;x^s)\rangle = \frac{1}{|\mathcal{S}|}\sum_{j\in\mathcal{S}}\mathcal{X}^M(j;x^s) \tag{6.27}$$

are averages over the index set $\mathcal{S}$, with cardinality $|\mathcal{S}|$. The set $\mathcal{S}$ of indexes included in the optimization is decided on the behavior of the model $\mathcal{X}^M(j;x^s)$ for different source locations. We show below, with numerical simulations, that the higher modes may not distinguish between different source cross-ranges, as they are most affected by the random medium. If $\mathcal{X}^M(j;x^s)$ does not show sensitivity to x^s, we exclude j from the set $\mathcal{S}$.

It is easy to infer from (6.25) that at long ranges, where $Z \gg L_e$, we cannot estimate the cross-range of the source. This is because $U_{jl} \approx 1/N(\omega_o)$ and $\mathcal{X}^M$ becomes essentially independent of x^s, as confirmed by the numerical experiments given below. However, the range estimation works at such long distances, as shown in the previous section.

Since it is only $\phi_l^2(x^s)$ that appears in the full aperture model (6.25), we cannot determine x^s uniquely, but find instead two possible cross-ranges, symmetric with respect to the axis of the waveguide. The general model (6.24) may suggest that we can resolve this ambiguity with partial apertures because of the coherent terms (the sum over $q \neq q'$ in (6.24)). However, these terms decay exponentially with the source range, and they are not expected to improve the estimation much. In fact, the numerical results show that partial apertures make the cross-range estimation quite difficult.

6.2.2. Numerical results. We present here cross-range estimation results in the same setup as in section 6.1.3. The unknown source is at $\vec{x}_\star = (5\lambda_c, 0)$ at unscaled range $z_{\mathcal{A}} = 494\lambda_c$ from the array.

We begin in Figure 6.5 with an illustration of the model function $\mathcal{X}^M(j;x^s)$, for a medium with $\varepsilon = 2\%$ fluctuations, at central frequency 2.69kHz, bandwidth 0.375kHz, and full aperture. This is the case considered in plot (i) of Figure 3.4, where both matched field and CINT give good results at full aperture but not at partial aperture (Figure 3.5). We plot $\mathcal{X}^M(j;x^s)$ for various source cross-ranges. Note the different oscillatory patterns for various x^s, and at the lower index of the

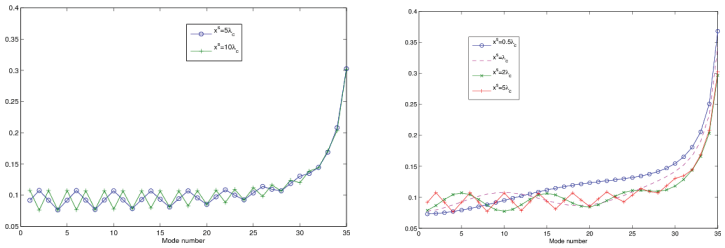

FIG. 6.5. *$\mathcal{X}^M(j;x^s)$ for $\varepsilon = 2\%$, central frequency 2.69kHz, bandwidth 0.375kHz, and full aperture. In the left plot we compare $\mathcal{X}^M(j;x^s)$ for $x^s = 5\lambda_c$ and $10\lambda_c$. On the right we take more values of x^s, equal to $0.5\lambda_c$, λ_c, $2\lambda_c$, and $5\lambda_c$, respectively.*

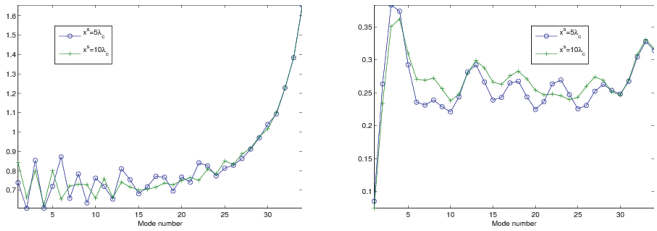

FIG. 6.6. *$\mathcal{X}^M(j;x^s)$ for $x^s = 5\lambda_c$ and $10\lambda_c$ for $\varepsilon = 2\%$, central frequency 2.69kHz, bandwidth 0.375kHz, and partial aperture. Left: $\mathcal{A} = [0, 12\lambda_c]$. Right: $\mathcal{A} = [0, 4\lambda_c]$.*

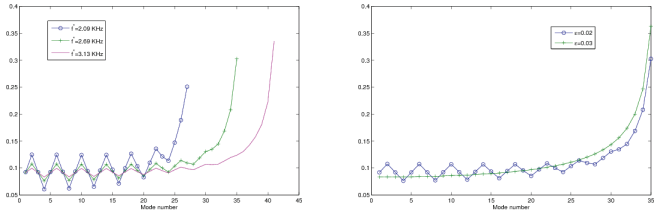

FIG. 6.7. *$\mathcal{X}^M(j;x^s)$ for $x^s = 5\lambda_c$ and full aperture. The left plot is at $\varepsilon = 2\%$ for central frequencies 2.09kHz, 2.69kHz, and 3.13kHz, respectively. The right plot is for central frequency 2.69kHz and $\varepsilon = 2\%$ and 3%. The bandwidth is 0.375kHz.*

modes, which are included in the set $\mathcal{S}$ used in the optimization. It is because of these different oscillatory patterns that we can estimate the source cross-range, independent of where it is in the interval $(0, X)$.

The plots of $\mathcal{X}^M(j;x^s)$ for partial apertures are in Figure 6.6, where $x^s = 5\lambda_c$ and $10\lambda_c$. They show that as we reduce the aperture, the cross-range estimation becomes ambiguous because the oscillations of $\mathcal{X}^M$ corresponding to different source locations are similar.

In Figure 6.7, we show the effect of the random medium on the model function $\mathcal{X}^M(j;x^s)$. Here we fix $x^s = x_\star = 5\lambda_c$ and plot in the left picture how $\mathcal{X}^M(j;x^s)$ changes as we increase the central frequency from 2.09kHz to 3.13kHz. In the right plot we fix the central frequency at 2.69kHz but increase ε from 2% to 3%. We note that as we increase the frequency and/or ε, the oscillatory pattern of $\mathcal{X}^M(j;x^s)$ is damped due to the stronger effect of the random medium. In fact, $\mathcal{X}^M(j;x^s)$ becomes less and less sensitive to x^s and the cross-range estimation becomes more and more ambiguous.

Figures 6.8–6.9 give the cross-range estimation results. We note that aside from

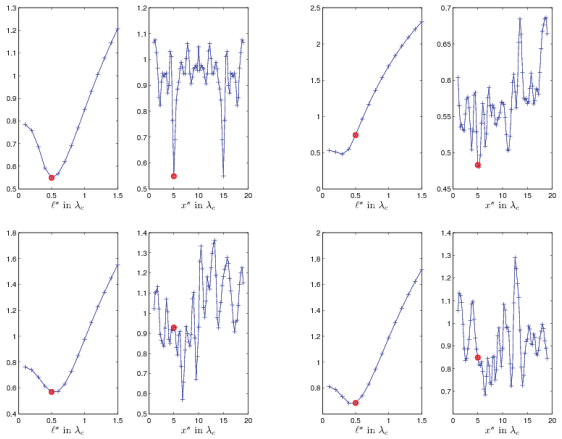

FIG. 6.8. *Cross-range estimation results at* $\varepsilon = 2\%$*, central frequency* $2.69kHz$*, and bandwidth* $0.375kHz$*. We plot the objective function* $\mathbb{O}$ *versus* x^s *and* ℓ^s*. Top left: full aperture* $\mathcal{A} = [0, 20\lambda_c]$*. Top right:* $\mathcal{A} = [0, 12\lambda_c]$*. Bottom left:* $\mathcal{A} = [0, 8\lambda_c]$*. Bottom right:* $\mathcal{A} = [0, 4\lambda_c]$*.*

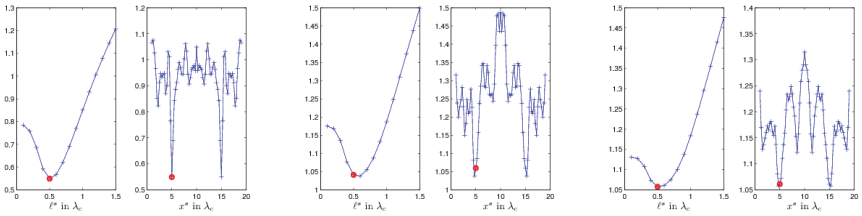

FIG. 6.9. *Full aperture cross-range estimation results at* $\varepsilon = 2\%$ *and bandwidth* $0.375kHz$*. The central frequency is* $2.69kHz$ *in the left plot,* $2.99kHz$ *in the middle plot, and* $3.13kHz$ *in the right plot.*

$x_\star$, we can also estimate the correlation function, although this is better done in conjunction with the range estimation. Here we use the true Gaussian model of the correlation function and we illustrate the estimation of the correlation length ℓ^s. The estimation of the amplitude parameter α^s appears to be ambiguous.

Figure 6.8 is at $\varepsilon = 2\%$, central frequency 2.69kHz, and bandwidth 0.375kHz, where matched field and CINT work at full aperture (case (i) in Figure 3.4) but not at partial aperture (Figure 3.5). The top left picture in Figure 6.8 shows the estimation at full aperture. The true values of the estimation parameters are indicated by a circle. The estimation returns the correct correlation length and source cross-range, except for the ghost that is symmetric with respect to the wave guide axis, as expected from the theory. The ghost is removed at partial apertures because there is still enough coherence in the data (recall the discussion at the end of section 6.2.1). However, we note that the estimation becomes more difficult as we reduce the aperture, and it is ambiguous at $\mathcal{A} = [0, 4\lambda_c]$ (bottom right plot). This is expected from the behavior of $\mathcal{X}^M(j; x^s)$ illustrated in Figure 6.5.

Figure 6.9 shows cross-range estimation results at full aperture for bandwidth 0.375kHz and central frequencies 2.69kHz, 2.99kHz, and 3.13kHz. These are cases (i), (ii), and (iii) in Figure 3.4. The cross-range estimation works well, but we note that the ratio of the peak and minimum of the objective function $\mathbb{O}(\vec{x}^s)$ approaches one

as we increase the frequency, indicating that the estimation becomes more difficult. This is expected from the behavior of the model $\mathcal{X}^M$ illustrated in Figure 6.7.

7. Summary. In this paper we study with analysis and numerical simulations the problem of source localization in random waveguides, given measurements of the acoustic pressure at a remote array $\mathcal{A}$ of receivers. We describe in detail the deterioration of coherent source localization methods, due to cumulative strong wave scattering by the random inhomogeneities in the waveguide, and introduce a novel incoherent source localization approach.

We consider three coherent methods: synthetic back propagation of the time reversed array data in deterministic (unperturbed) waveguides; matched field; and CINT. The first method is the same as time reversal, when the source localization occurs in unperturbed waveguides. Time reversal works well in random waveguides, but it cannot be used for source localization, because we cannot implement the back propagation in the true medium, which is unknown. We find that synthetic back propagation in the unperturbed waveguide is not useful because it lacks statistical stability with respect to the realization of the medium. Explicitly, we show that the mean of the estimation function focuses at the correct location, but its amplitude decays exponentially with range and central frequency. This is because the wave field loses its coherence rapidly (exponentially), and the energy is transferred to the fluctuations, the incoherent field. Consequently, the relative standard deviation of the estimation function is very large and the method is unstable.

The matched field and coherent interferometric source localization functions are not useful for localizing sources at long ranges either. Both methods use cross-correlations of the array data, which have a nontrivial long range mean. However, since they do not account for the strong dispersive effect induced by scattering in the waveguide, they do not focus at the source location.

To localize the source from almost incoherent array data, we need to systematically exploit the dispersive effect induced by the random medium. This requires a mathematical model, which allows us to restate the problem as one of parameter estimation for the source coordinates and possibly the correlation function of the random fluctuations of the wave speed. We use here the asymptotic model derived in [14, 9, 12, 11]. The asymptotics is in the amplitude scale of the fluctuations, which is typically 1%–3% in underwater acoustics [10], and for long distances of propagation. We show how to use the model to formulate a statistically stable incoherent source localization approach. We analyze the method in detail and assess its performance with extensive numerical simulations.

Appendix A. Time reversal refocusing in unperturbed waveguides. We begin with expression (5.5) of the time reversal function. Based on the $O(1/B)$ support of $f_B(t)$, we can change variables,

$$Z^s - Z = -\varepsilon^{2-\sigma}\eta^s, \quad \text{i.e.,} \quad z^s = z_{\mathcal{A}} - Z^s/\varepsilon^2 = \varepsilon^{-\sigma}\eta^s,$$

and obtain

$$\mathcal{I}_o^{TR}(x^s, \varepsilon^{-\sigma}\eta^s) \approx \frac{1}{4}\sum_{j=1}^{N(\omega_o)} \phi_j(x_\star)\phi_j(x^s)e^{-i\beta_j(\omega_o)\eta^s/\varepsilon^\sigma}\,\overline{f_B}\left(-\beta_j'(\omega_o)\eta^s\right). \tag{A.1}$$

This is a sum of highly oscillatory terms, and we expect that when $N(\omega_o)$ is large

enough, there will be a lot of cancellations unless $\beta_j(\omega_o)\eta^s \sim \eta^s/\lambda_o \leq O(\varepsilon^\sigma)$. Indeed,

$$\begin{aligned}
\mathcal{I}_o^{TR}(x^s, \varepsilon^\sigma \eta^s) &\approx \frac{1}{\lambda_o N} \sum_{j=1}^{N} \sin\left(\frac{j}{N}\frac{2\pi x^s}{\lambda_o}\right) \sin\left(\frac{j}{N}\frac{2\pi x_\star}{\lambda_o}\right) \\
&\quad \times e^{-i\varepsilon^{-\sigma}\eta^s \frac{2\pi}{\lambda_o}\sqrt{1-\frac{j^2}{N^2}}} \overline{f_B}\left(\frac{-\eta^s}{c_o\sqrt{1-\frac{j^2}{N^2}}}\right) \\
&\approx \frac{1}{2\lambda_o}\int_0^1 d\xi \left[\cos\left(\xi\frac{2\pi(x^s - x_\star)}{\lambda_o}\right) - \cos\left(\xi\frac{2\pi(x^s + x_\star)}{\lambda_o}\right)\right] \\
&\quad \times e^{-i\frac{2\pi\varepsilon^{-\sigma}\eta^s}{\lambda_o}\sqrt{1-\xi^2}} \overline{f_B}\left(\frac{-\eta^s}{c_o\sqrt{1-\xi^2}}\right)
\end{aligned}$$

when $N = N(\omega_o) = \lfloor 2X/\lambda_o \rfloor \gtrsim \varepsilon^{-\sigma} \gg 1$, and we can interpret the sum over $\xi_j = j/N$ as a Riemann sum for the integral over $\xi \in (0,1)$. Then, it follows from the method of stationary phase [3, Chapter 6] that $\mathcal{I}_o^{TR}$ is large for $\eta^s/\lambda_o \sim \varepsilon^\sigma$ so that $z^s \sim \lambda_o$. At the true source range ($z^s = 0$), we have

$$\begin{aligned}
\mathcal{I}_o^{TR}(x^s, 0) &\approx \frac{\overline{f_B}(0)}{4} \sum_{j=1}^{N(\omega_o)} \phi_j(x_\star)\phi_j(x^s) \\
&\approx \frac{\overline{f_B}(0)}{2\lambda_o}\int_0^1 d\xi \left[\cos\left(\xi\frac{2\pi(x^s - x_\star)}{\lambda_o}\right) - \cos\left(\xi\frac{2\pi(x^s + x_\star)}{\lambda_o}\right)\right] \\
&\approx \frac{\overline{f_B}(0)}{2\lambda_o} \operatorname{sinc}\left[\frac{2\pi(x^s - x_\star)}{\lambda_o}\right] \qquad \text{(A.2)}
\end{aligned}$$

in the limit $N(\omega_o) \gg 1$. ∎

Appendix B. Proof of Proposition 6.1. Recall model (4.20) of the array data, and set $z_{\mathcal{A}} = Z/\varepsilon^2$, to obtain from (6.6)

$$\widehat{P}_j(\omega, z_{\mathcal{A}}) \approx \frac{\widehat{f^\varepsilon}(\omega)}{2} \sum_{q,l=1}^{N(\omega_o)} \mathcal{M}_{jq}\sqrt{\frac{\beta_l(\omega_o)}{\beta_q(\omega_o)}}\phi_l(x_\star) T_{ql}^\varepsilon(\omega, Z) e^{i\beta_q(\omega)Z/\varepsilon^2}. \qquad \text{(B.1)}$$

Then,

$$\mathcal{R}(\zeta, j) = \int_{|\omega-\omega_o|\leq \varepsilon^\sigma B} \frac{d\omega}{2\pi}\widehat{\mathcal{R}}(\omega, \zeta, j), \qquad \text{(B.2)}$$

where

$$\widehat{\mathcal{R}}(\omega, \zeta, j) = \int_{|\omega-\omega'|\leq \varepsilon^2\Omega} \frac{d\omega'}{2\pi}\widehat{P}_j(\omega, z_{\mathcal{A}})\overline{\widehat{P}_j}(\omega', z_{\mathcal{A}}) \qquad \text{(B.3)}$$

is given by

$$\begin{aligned}
\widehat{\mathcal{R}}(\omega, \zeta, j) &\approx \frac{\varepsilon^2}{4} \sum_{q,l,q',l'=1}^{N(\omega_o)} \mathcal{M}_{jq}\mathcal{M}_{jq'}\sqrt{\frac{\beta_l(\omega_o)\beta_{l'}(\omega_o)}{\beta_q(\omega_o)\beta_{q'}(\omega_o)}}\phi_l(x_\star)\phi_{l'}(x_\star) e^{i\left[\beta_q(\omega)-\beta_{q'}(\omega)\right]Z/\varepsilon^2} \\
&\quad \times \int_{-\Omega}^{\Omega} \frac{d\widetilde{h}}{2\pi}\,\widehat{f^\varepsilon}\left(\omega + \varepsilon^2\widetilde{h}/2\right)\overline{\widehat{f^\varepsilon}}\left(\omega - \varepsilon^2\widetilde{h}/2\right) T_{ql}^\varepsilon\left(\omega + \varepsilon^2\widetilde{h}/2, Z\right) \\
&\quad \times \overline{T_{q'l'}^\varepsilon}\left(\omega - \varepsilon^2\widetilde{h}/2, Z\right) e^{i\widetilde{h}Z\left[\beta_q'(\omega)+\beta_{q'}'(\omega)\right]/2 - i\widetilde{h}\zeta\beta_j'(\omega)} \qquad \text{(B.4)}
\end{aligned}$$

after the change of variables $(\omega+\omega')/2 \rightsquigarrow \omega$ and $\omega-\omega' \rightsquigarrow \varepsilon^2\widetilde{h}$. Taking expectations and using Lemma 5.2,

(B.5)
$$E\left\{\widehat{\mathcal{R}}(\omega,\zeta,j)\right\} \approx \frac{\varepsilon^2}{4}\sum_{q,l=1}^{N(\omega_o)} \mathcal{M}_{jq}^2 \frac{\beta_l(\omega_o)}{\beta_q(\omega_o)}\phi_l^2(x_\star)\int d\tau\, \mathcal{W}_q^{(l)}(\omega,\tau,Z)\Psi(\omega,\beta_j'(\omega)\zeta-\tau),$$

where

$$\Psi(\omega,t) = \int_{-\Omega}^{\Omega}\frac{d\widetilde{h}}{2\pi}\,\widehat{f}^{\varepsilon}\left(\omega+\frac{\varepsilon^2\widetilde{h}}{2}\right)\overline{\widehat{f}^{\varepsilon}}\left(\omega-\frac{\varepsilon^2\widetilde{h}}{2}\right)e^{-i\widetilde{h}t}, \tag{B.6}$$

and we neglect the exponentially decaying terms in Z.

Now, let us evaluate (B.6) using the definition (4.21) of $\widehat{f}^{\varepsilon}$ and for $\sigma\in(1,2]$. For broad band pulses, we can approximate

$$\widehat{f}^{\varepsilon}\left(\omega\pm\frac{\varepsilon^2\widetilde{h}}{2}\right) = \frac{1}{\varepsilon^{\sigma}}\widehat{f}_B\left(\frac{\omega-\omega_o}{\varepsilon^{\sigma}}\pm\frac{\varepsilon^{2-\sigma}\widetilde{h}}{2}\right) \approx \frac{1}{\varepsilon^{\sigma}}\widehat{f}_B\left(\frac{\omega-\omega_o}{\varepsilon^{\sigma}}\right)$$

and obtain

$$\Psi(\omega,t) \approx \frac{\Omega\varepsilon^{-2\sigma}}{\pi}\left|\widehat{f}_B\left(\frac{\omega-\omega_o}{\varepsilon^{\sigma}}\right)\right|^2 \operatorname{sinc}(\Omega t), \qquad \sigma\in(1,2). \tag{B.7}$$

In the narrow band case $\sigma=2$,

$$\widehat{f}^{\varepsilon}\left(\omega\pm\frac{\varepsilon^2\widetilde{h}}{2}\right) = \frac{1}{\varepsilon^{2}}\widehat{f}_B\left(\frac{\omega-\omega_o}{\varepsilon^{2}}\pm\frac{\widetilde{h}}{2}\right)$$

and

$$\begin{aligned}\Psi(\omega,t) &\approx \frac{1}{\varepsilon^4}\int dt_1\int dt_2 f_B(t_1)\overline{f_B(t_2)}e^{i(\omega-\omega_o)(t_1-t_2)/\varepsilon^2}\int_{-\Omega}^{\Omega}\frac{d\widetilde{h}}{2\pi}\,e^{i\widetilde{h}[(t_1+t_2)/2-t]}\\ &= \frac{\Omega\varepsilon^{-4}}{\pi}\int dt_1\int dt_2 f_B(t_1)\overline{f_B(t_2)}e^{i(\omega-\omega_o)(t_1-t_2)/\varepsilon^2}\operatorname{sinc}\left[\Omega\left(\frac{t_1+t_2}{2}-t\right)\right].\end{aligned} \tag{B.8}$$

Thus, the theoretical expected model of (6.8) is given by

$$\begin{aligned}E\{\mathcal{R}(\zeta,j)\} &\approx \frac{\varepsilon^{2-2\sigma}}{4}\sum_{q,l=1}^{N(\omega_o)}\mathcal{M}_{jq}^2\frac{\beta_l(\omega_o)}{\beta_q(\omega_o)}\phi_l^2(x_\star)\\ &\quad\times\int\frac{d\omega}{2\pi}\int d\tau\mathcal{W}_q^{(l)}(\omega,\tau,Z)\left|\widehat{f}_B\left(\frac{\omega-\omega_o}{\varepsilon^{\sigma}}\right)\right|^2\frac{\Omega}{\pi}\operatorname{sinc}\left[\Omega\left(\beta_j'(\omega)\zeta-\tau\right)\right]\\ &\approx \frac{\varepsilon^{2-\sigma}\|f_B\|^2}{4}\sum_{q,l=1}^{N(\omega_o)}\mathcal{M}_{jq}^2\frac{\beta_l(\omega_o)}{\beta_q(\omega_o)}\phi_l^2(x_\star)\mathcal{W}_q^{(l)}(\omega_o,\beta_j'(\omega_o)\zeta,Z)\end{aligned} \tag{B.9}$$

in broad band and by

$$
\begin{aligned}
E\left\{\mathcal{R}(\zeta,j)\right\} &\approx \frac{\varepsilon^{-2}}{4}\sum_{q,l=1}^{N(\omega_o)} \mathcal{M}_{jq}^2 \frac{\beta_l(\omega_o)}{\beta_q(\omega_o)}\phi_l^2(x_\star)\int \frac{d\omega}{2\pi}\int d\tau\, \mathcal{W}_q^{(l)}(\omega,\tau,Z)\\
&\quad\times \int dt_1 \int dt_2\, f_B(t_1)\,\overline{f_B}\,(t_2) e^{i(\omega-\omega_o)(t_1-t_2)/\varepsilon^2}\\
&\quad\times \frac{\Omega}{\pi}\,\mathrm{sinc}\left[\Omega\left(\frac{t_1+t_2}{2}+\tau-\beta_j'(\omega)\zeta\right)\right]\\
&\approx \frac{1}{4}\sum_{q,l=1}^{N(\omega_o)} \mathcal{M}_{jq}^2 \frac{\beta_l(\omega_o)}{\beta_q(\omega_o)}\phi_l^2(x_\star)\int d\tau\, \mathcal{W}_q^{(l)}(\omega_o,\beta_j'(\omega_o)\zeta-\tau,Z)\\
&\quad\times \int d\widetilde{t}\,\frac{B}{\pi}\,\mathrm{sinc}\left(B\widetilde{t}\right) f_B\left(\tau+\frac{\widetilde{t}}{2}\right)\overline{f_B}\left(\tau-\frac{\widetilde{t}}{2}\right) \qquad \text{(B.10)}
\end{aligned}
$$

in narrow band. □

Appendix C. The fourth order multifrequency moments of the transfer matrix. We wish to calculate the fourth order multifrequency moments

$$E\left\{T_{jm}^\varepsilon(\omega+\varepsilon^2 h,Z)\overline{T_{ln}^\varepsilon}(\omega-\varepsilon^2\tilde{\omega},Z)\overline{T_{J\mathcal{M}}^\varepsilon}(\omega-\varepsilon^2\tilde{\omega}',Z)T_{L\mathcal{N}}^\varepsilon(\omega+\varepsilon^2 h',Z)\right\}$$

for frequency offsets h, h', $\tilde{\omega}$, and $\tilde{\omega}'$ of order one. For this, we use that T^ε satisfies stochastic equations (4.18) and write that

$$
\begin{aligned}
e^{ihz\beta_j'}\frac{\partial}{\partial z}T_{jm}^\varepsilon &= \frac{\partial}{\partial z}\mathbb{T}_{jm}^\varepsilon - ih\beta_j'\mathbb{T}_{jm}^\varepsilon = \frac{i\omega^2}{2c_o^2\varepsilon}\sum_{p=1}^N \mathbb{T}_{pm}^\varepsilon \frac{C_{jp}(z/\varepsilon^2)}{\sqrt{\beta_p\beta_j}}e^{i(\beta_p-\beta_j)z/\varepsilon^2}\\
&\quad + \frac{i\omega^4}{4c_o^4}\sum_{p=1}^N \mathbb{T}_{pm}^\varepsilon \sum_{l'>N}\int_{-\infty}^\infty ds \frac{C_{jl'}(z/\varepsilon^2)C_{pl'}(z/\varepsilon^2+s)}{\beta_{l'}\sqrt{\beta_p\beta_j}}e^{-\beta_{l'}|s|+i\beta_p s+i(\beta_p-\beta_j)z/\varepsilon^2} \qquad \text{(C.1)}
\end{aligned}
$$

for $z>0$, where

$$\mathbb{T}_{jm}^\varepsilon(\omega+\varepsilon^2 h,z) = e^{ihz\beta_j'(\omega)}T_{jm}^\varepsilon(\omega+\varepsilon^2 h,z). \qquad \text{(C.2)}$$

At $z=0$ we have the initial conditions

$$\mathbb{T}_{jm}^\varepsilon(\omega+\varepsilon^2 h,0) = T_{jm}^\varepsilon(\omega+\varepsilon^2 h,0) = \delta_{jm}. \qquad \text{(C.3)}$$

Then, we can write

$$
\begin{aligned}
&E\left\{T_{jm}^\varepsilon(\omega+\varepsilon^2 h,z)\overline{T_{ln}^\varepsilon}(\omega-\varepsilon^2\tilde{\omega},z)\overline{T_{J\mathcal{M}}^\varepsilon}(\omega-\varepsilon^2\tilde{\omega}',z)T_{L\mathcal{N}}^\varepsilon(\omega+\varepsilon^2 h',z)\right\}\\
&\quad = e^{-i(h\beta_j'+\tilde{\omega}\beta_l'+\tilde{\omega}'\beta_J'+h'\beta_L')z}E\left\{\mathbb{V}_{jlJL}^\varepsilon(\omega,h,h',\tilde{\omega},\tilde{\omega}')\right\}, \qquad \text{(C.4)}
\end{aligned}
$$

where we let

$$\mathbb{V}_{jlJL}^\varepsilon(\omega,h,h',\tilde{\omega},\tilde{\omega}') = \mathbb{T}_{jm}^\varepsilon(\omega+\varepsilon^2 h,Z)\overline{\mathbb{T}_{ln}^\varepsilon}(\omega-\varepsilon^2\tilde{\omega},z)\overline{\mathbb{T}_{J\mathcal{M}}^\varepsilon}(\omega-\varepsilon^2\tilde{\omega}',Z)\mathbb{T}_{L\mathcal{N}}^\varepsilon(\omega+\varepsilon^2 h',z) \qquad \text{(C.5)}$$

and suppress the indexes m, n, $\mathcal{M}$, and $\mathcal{N}$ in the notation. These indexes are parameters in the differential equations (C.1), but they influence the initial conditions (C.3).

The stochastic system of differential equations for $\mathbb{V}^\varepsilon_{jlJL}$ follows from (C.1), and we write it in compact form as

$$\begin{aligned} \frac{\partial}{\partial z}\mathbb{V}^\varepsilon_{jlJL} &= \frac{1}{\varepsilon}\mathbb{F}_{jlJL} + \mathbb{G}_{jlJL}, \qquad z>0, \\ \mathbb{V}^\varepsilon_{jlJL}\big|_{z=0} &= \delta_{jm}\delta_{ln}\delta_{J\mathcal{M}}\delta_{L\mathcal{N}}, \end{aligned} \tag{C.6}$$

where

$$\begin{aligned} \mathbb{F}_{jlJL} = \frac{i\omega^2}{2c_o^2}\sum_{p=1}^{N}\Bigg[&\frac{C_{jp}(z/\varepsilon^2)}{\sqrt{\beta_p\beta_j}}e^{i(\beta_p-\beta_j)z/\varepsilon^2}\mathbb{V}^\varepsilon_{plJL} - \frac{C_{lp}(z/\varepsilon^2)}{\sqrt{\beta_p\beta_l}}e^{-i(\beta_p-\beta_l)z/\varepsilon^2}\mathbb{V}^\varepsilon_{jpJL} \\ &- \frac{C_{Jp}(z/\varepsilon^2)}{\sqrt{\beta_p\beta_J}}e^{-i(\beta_p-\beta_J)z/\varepsilon^2}\mathbb{V}^\varepsilon_{jlpL} + \frac{C_{Lp}(z/\varepsilon^2)}{\sqrt{\beta_p\beta_L}}e^{i(\beta_p-\beta_L)z/\varepsilon^2}\mathbb{V}^\varepsilon_{jlJp}\Bigg] \end{aligned} \tag{C.7}$$

and

$$\begin{aligned} \mathbb{G}_{jlJL} = {} & i\left[h\beta'_j + \tilde{\omega}\beta'_l + \tilde{\omega}'\beta'_J + h'\beta'_L\right]\mathbb{V}^\varepsilon_{jlJL} \\ & + \frac{i\omega^4}{4c_o^4}\sum_{p=1}^{N}\sum_{l'>N}\int_{-\infty}^{\infty} ds\, e^{-\beta_{l'}|s|}\frac{C_{pl'}(z/\varepsilon^2+s)}{\beta_{l'}} \\ & \times\Bigg[\frac{C_{jl'}(z/\varepsilon^2)}{\sqrt{\beta_p\beta_j}}e^{i\beta_p s+i(\beta_p-\beta_j)z/\varepsilon^2}\mathbb{V}^\varepsilon_{plJL} - \frac{C_{ll'}(z/\varepsilon^2)}{\sqrt{\beta_p\beta_j}}e^{-i\beta_p s-i(\beta_p-\beta_l)z/\varepsilon^2}\mathbb{V}^\varepsilon_{jpJL} \\ & - \frac{C_{Jl'}(z/\varepsilon^2)}{\sqrt{\beta_p\beta_J}}e^{-i\beta_p s-i(\beta_p-\beta_J)z/\varepsilon^2}\mathbb{V}^\varepsilon_{jlpL} + \frac{C_{Ll'}(z/\varepsilon^2)}{\sqrt{\beta_p\beta_L}}e^{i\beta_p s+i(\beta_p-\beta_L)z/\varepsilon^2}\mathbb{V}^\varepsilon_{jlJp}\Bigg]. \end{aligned} \tag{C.8}$$

We are almost ready to apply the diffusion approximation theorem [11, Theorem 6.5], in order to obtain $E\left\{\mathbb{V}^\varepsilon_{jlJL}\right\}$ in the limit $\varepsilon\to 0$. We need to do one more step, and write (C.6) as a system of differential equations for vector $\mathbf{V}^\varepsilon\in\mathbb{R}^{2N^4}$, with components

$$\begin{aligned} V^\varepsilon_{(L-1)N^3+(J-1)N^2+(l-1)N+j} &= \operatorname{Re}\mathbb{V}^\varepsilon_{jlJL}, \\ V^\varepsilon_{N^4+(L-1)N^3+(J-1)N^2+(l-1)N+j} &= \operatorname{Im}\mathbb{V}^\varepsilon_{jlJL}. \end{aligned} \tag{C.9}$$

Equations (C.6) become

$$\frac{\partial}{\partial z}\mathbf{V}^\varepsilon = \frac{1}{\varepsilon}\mathcal{F}\left[\nu\left(\cdot,\frac{z}{\varepsilon^2}\right),\frac{z}{\varepsilon^2}\right]\mathbf{V}^\varepsilon + \mathcal{G}\left[\nu\left(\cdot,\frac{z}{\varepsilon^2}\right),\frac{z}{\varepsilon^2}\right]\mathbf{V}^\varepsilon, \tag{C.10}$$

with matrices $\mathcal{F},\mathcal{G}\in\mathbb{R}^{2N^4\times 2N^4}$ following obviously from (C.7) and (C.8).

We obtain from [11, Theorem 6.5] that as $\varepsilon\to 0$, $\mathbf{V}^\varepsilon$ converges in distribution to the diffusion Markov process $\mathbf{V}$ with generator $\mathbb{Q}$ given by

$$\begin{aligned} \mathbb{Q}\varphi(\mathbf{v}) = {} & \lim_{\bar{Z}\to\infty}\frac{1}{\bar{Z}}\int_0^{\bar{Z}} ds\int_0^\infty dz E\{\mathcal{F}(\nu(\cdot,0),s)\mathbf{v}\cdot\nabla_{\mathbf{v}}[\mathcal{F}(\nu(\cdot,z),s+z)\mathbf{v}\cdot\nabla_{\mathbf{v}}\varphi(\mathbf{v})]\} \\ & + \lim_{\bar{Z}\to\infty}\frac{1}{\bar{Z}}\int_0^{\bar{Z}} ds E\{\mathcal{G}(\nu(\cdot,0),s)\mathbf{v}\cdot\nabla_{\mathbf{v}}\varphi(\mathbf{v})\} \end{aligned} \tag{C.11}$$

for an arbitrary smooth function φ. To get the limit of $E\left\{\mathbb{V}^\varepsilon_{jlJL}\right\}$ as $\varepsilon\to 0$, it suffices to compute the action of $\mathbb{Q}$ on $\varphi(\mathbf{v})=v_q$ and $\varphi(\mathbf{v})=v_{q+N^4}$, where $q=(L-1)N^3+(J-1)N^2+(l-1)N+j$. Then, the result follows from Kolmogorov's backward equation [7].

We obtain after tedious but straightforward calculations that

$$\lim_{\varepsilon\to 0} E\left\{\mathbb{V}^{\varepsilon}_{jlJL}\right\} = \mathcal{V}_{jlJL}(\omega,h,h',\tilde{\omega},\tilde{\omega}',z), \tag{C.12}$$

where

$$\begin{aligned}\frac{\partial}{\partial z}\mathcal{V}_{jlJL} = &\left[i\left(h\beta'_j+\tilde{\omega}\beta'_l+\tilde{\omega}'\beta'_J+h'\beta'_L\right)+Q_{jlJL}\right]\mathcal{V}_{jlJL} - (1-\delta_{jL})\Gamma^{(c)}_{jL}\mathcal{V}_{LlJj}\\ &-(1-\delta_{jL})\Gamma^{(c)}_{Jl}\mathcal{V}_{jJlL}+\delta_{lj}\sum_{p\neq j,\,p=1}^{N}\Gamma^{(c)}_{pj}\mathcal{V}_{ppJL}+\delta_{Jj}\sum_{p\neq j,\,p=1}^{N}\Gamma^{(c)}_{pj}\mathcal{V}_{plpL}\\ &+\delta_{lL}\sum_{p\neq l,\,p=1}^{N}\Gamma^{(c)}_{pl}\mathcal{V}_{jpJp}+\delta_{JL}\sum_{p\neq J,\,p=1}^{N}\Gamma^{(c)}_{pJ}\mathcal{V}_{jlpp}\end{aligned} \tag{C.13}$$

for $z>0$, and

$$\begin{aligned}Q_{jlJL} = &\frac{1}{2}\left(\Gamma^{(c)}_{jj}+\Gamma^{(c)}_{ll}+\Gamma^{(c)}_{JJ}+\Gamma^{(c)}_{LL}\right)-\frac{1}{2}\left(\Gamma^{(1)}_{jj}+\Gamma^{(1)}_{ll}+\Gamma^{(1)}_{JJ}+\Gamma^{(1)}_{LL}\right)\\ &+\Gamma^{(1)}_{jl}+\Gamma^{(1)}_{jJ}+\Gamma^{(1)}_{lL}+\Gamma^{(1)}_{JL}-\Gamma^{(1)}_{lJ}-\Gamma^{(1)}_{jL}\\ &+\frac{i}{2}\left(\Gamma^{(s)}_{jj}+\Gamma^{(s)}_{LL}-\Gamma^{(s)}_{ll}-\Gamma^{(s)}_{JJ}\right)+i\left(\kappa_j+\kappa_L-\kappa_l-\kappa_J\right).\end{aligned} \tag{C.14}$$

The initial conditions at $z=0$ are

$$\mathcal{V}_{jlJL}(\omega,h,h',\tilde{\omega},\tilde{\omega}',z=0) = \delta_{jm}\delta_{ln}\delta_{J\mathcal{M}}\delta_{L\mathcal{N}}. \tag{C.15}$$

Proposition D.1 now follows easily from (C.13)–(C.15). ∎

Appendix D. Proof of Proposition 6.4. We need the following result.

PROPOSITION D.1. *Consider arbitrary indexes $j,l,l',n,n' = 1,\dots,N(\omega)$. As $\varepsilon\to 0$, we have*

$$\begin{aligned}&E\left\{T^{\varepsilon}_{jl}\left(\omega+\frac{\varepsilon^2(\tilde{\omega}+\widetilde{h})}{2},Z\right)\overline{T^{\varepsilon}_{jl'}}\left(\omega-\frac{\varepsilon^2(\tilde{\omega}-\widetilde{h})}{2},Z\right)\right.\\ &\left.\times\,\overline{T^{\varepsilon}_{jn}}\left(\omega-\frac{\varepsilon^2(\tilde{\omega}'+\widetilde{h})}{2},Z\right)T^{\varepsilon}_{jn'}\left(\omega+\frac{\varepsilon^2(\tilde{\omega}'-\widetilde{h})}{2},Z\right)\right\}\\ &\to e^{-i(\tilde{\omega}+\tilde{\omega}')\beta'_jZ}\mathcal{V}_{jjjj}(\omega,\tilde{\omega},\tilde{\omega}',\widetilde{h},Z),\end{aligned} \tag{D.1}$$

where $\{\mathcal{V}_{jjqq}\}_{j,q=1,\dots,N(\omega)}$ and $\{\mathcal{V}_{jqjq}\}_{j\neq q=1,\dots,N(\omega)}$ satisfy the closed system of equations

$$\begin{aligned}\frac{\partial}{\partial z}\mathcal{V}_{jjqq} = &\,i\left[\left(\frac{\tilde{\omega}+\tilde{\omega}'}{2}\right)(\beta'_j+\beta'_q)+\left(\frac{\tilde{\omega}-\tilde{\omega}'}{2}\right)(\beta'_j-\beta'_q)\right]\mathcal{V}_{jjqq}-\Gamma^{(c)}_{jq}\left[\mathcal{V}_{jqjq}+\mathcal{V}_{qjqj}\right]\\ &+\sum_{p\neq j,\,p=1}^{N}\Gamma^{(c)}_{pj}\left(\mathcal{V}_{ppqq}-\mathcal{V}_{jjqq}\right)+\sum_{p\neq q,\,p=1}^{N}\Gamma^{(c)}_{pq}\left(\mathcal{V}_{jjpp}-\mathcal{V}_{jjqq}\right)\\ &+\delta_{jq}\left[\sum_{p\neq j,\,p=1}^{N}\Gamma^{(c)}_{pj}\left(\mathcal{V}_{pjpj}-\mathcal{V}_{jjjj}\right)+\sum_{p\neq j,\,p=1}^{N}\Gamma^{(c)}_{pj}\left(\mathcal{V}_{jpjp}-\mathcal{V}_{jjjj}\right)\right],\\ &j,q=1,\dots,N(\omega_o),\end{aligned}$$

$$\frac{\partial}{\partial z}\mathcal{V}_{jqjq} = i\left[\left(\frac{\tilde\omega+\tilde\omega'}{2}\right)(\beta_j'+\beta_q') + \widetilde{h}(\beta_j'-\beta_q')\right]\mathcal{V}_{jqjq} - \Gamma_{jq}^{(c)}\left[\mathcal{V}_{jjqq}+\mathcal{V}_{qqjj}\right]$$
$$+\sum_{p\neq j,\,p=1}^{N}\Gamma_{pj}^{(c)}\left(\mathcal{V}_{pqpq}-\mathcal{V}_{jqjq}\right)+\sum_{p\neq q,\,p=1}^{N}\Gamma_{pq}^{(c)}\left(\mathcal{V}_{jpjp}-\mathcal{V}_{jqjq}\right), \qquad j\neq q,$$

for $z>0$ and initial conditions

$$\mathcal{V}_{jjqq}(\omega,\tilde\omega,\tilde\omega',\widetilde{h},z=0)=\delta_{jl}\delta_{jl'}\delta_{qn}\delta_{qn'},$$
$$\mathcal{V}_{jqjq}(\omega,\widetilde{h},\tilde\omega,\tilde\omega',\widetilde{h},z=0)=\delta_{jl}\delta_{ql'}\delta_{jn}\delta_{qn'}. \tag{D.2}$$

The proof is in Appendix C. Note that the initial conditions (D.2) are identically zero unless l,l',n,n' satisfy one of the following conditions:

$$l=l' \ \text{ and } \ n=n', \tag{D.3}$$
$$l=n\neq l'=n'. \tag{D.4}$$

This means that of all moments (D.1), only those with these indexes are not zero. Note also that in Proposition D.1 and in Appendix C we suppressed the initial condition notation in $\mathcal{V}_{jjjj}$. We restore it now by writing

$$\mathcal{V}_{jjjj}\rightsquigarrow\mathcal{V}_{jjjj}^{ll'nn'}.$$

We obtain from (6.20), Lemma 5.2, and Proposition D.1 that

$$V(\zeta,j)\approx\frac{\varepsilon^{3(2-\sigma)}}{4^2}\int_{-B}^{B}\frac{dh}{2\pi}\int_{-\Omega}^{\Omega}\frac{d\widetilde{h}}{2\pi}\int_{-\Omega}^{\Omega}\frac{d\tilde\omega}{2\pi}\int_{-\Omega}^{\Omega}\frac{d\tilde\omega'}{2\pi}e^{i(\tilde\omega+\tilde\omega')(Z-\zeta)\beta_j'(\omega_o)}$$
$$\times\widehat{f}_B\left(h+\frac{\varepsilon^{2-\sigma}}{2}(\tilde\omega+\widetilde{h})\right)\overline{\widehat{f}_B}\left(h-\frac{\varepsilon^{2-\sigma}}{2}(\tilde\omega-\widetilde{h})\right)$$
$$\times\overline{\widehat{f}_B}\left(h-\frac{\varepsilon^{2-\sigma}}{2}(\tilde\omega'+\widetilde{h})\right)\overline{\widehat{f}_B}\left(h+\frac{\varepsilon^{2-\sigma}}{2}(\tilde\omega'-\widetilde{h})\right)$$
$$\times\sum_{l,l',n,n'=1}^{N(\omega_o)}\frac{\sqrt{\beta_l\beta_{l'}\beta_n\beta_{n'}'}}{\beta_j^2}\phi_l(x_\star)\phi_{l'}(x_\star)\phi_n(x_\star)\phi_{n'}(x_\star)\mathcal{F}_{ll'nn'}(\omega_o+\varepsilon^\sigma h,\tilde\omega,\tilde\omega',\widetilde{h}),$$

where

$$\mathcal{F}_{ll'nn'}(\omega,\tilde\omega,\tilde\omega',\widetilde{h})=e^{-i(\tilde\omega+\tilde\omega')Z\beta_j'(\omega)}\left[\delta_{ll'}\delta_{nn'}+(1-\delta_{ll'})\delta_{ln}\delta_{l'n'}\right]\mathcal{V}_{jjjj}^{ll'nn'}\left(\omega,\tilde\omega,\tilde\omega',\widetilde{h},Z\right)$$
$$-e^{-i(\tilde\omega+\tilde\omega')Z\beta_j'(\omega)}\delta_{ll'}\delta_{nn'}\widehat{W}_j^{(l)}(\omega,\tilde\omega,Z)\widehat{W}_j^{(n)}(\omega,\tilde\omega',Z). \tag{D.5}$$

The expression of the variance becomes

$$V(\zeta,j)\approx\frac{\varepsilon^{3(2-\sigma)}}{16}\int_{-B}^{B}\frac{dh}{2\pi}\int_{-\Omega}^{\Omega}\frac{d\widetilde{h}}{2\pi}\int_{-\Omega}^{\Omega}\frac{d\tilde\omega}{2\pi}\int_{-\Omega}^{\Omega}\frac{d\tilde\omega'}{2\pi}e^{-i(\tilde\omega+\tilde\omega')\zeta\beta_j'(\omega_o)}$$
$$\times\widehat{f}_B\left(h+\frac{\varepsilon^{2-\sigma}}{2}(\tilde\omega+\widetilde{h})\right)\overline{\widehat{f}_B}\left(h-\frac{\varepsilon^{2-\sigma}}{2}(\tilde\omega-\widetilde{h})\right)$$
$$\times\overline{\widehat{f}_B}\left(h-\frac{\varepsilon^{2-\sigma}}{2}(\tilde\omega'+\widetilde{h})\right)\overline{\widehat{f}_B}\left(h+\frac{\varepsilon^{2-\sigma}}{2}(\tilde\omega'-\widetilde{h})\right)$$
$$\times\sum_{l,n=1}^{N(\omega_o)}\frac{\beta_l(\omega_o)\beta_n(\omega_o)}{\beta_j^2}\phi_l^2(x_\star)\phi_n^2(x_\star)$$
$$\times\left[\mathcal{V}_{jjjj}^{llnn}+(1-\delta_{ln})\mathcal{V}_{jjjj}^{lnln}-\widehat{W}_j^{(l)}(\omega_o,\tilde\omega,Z)\widehat{W}_j^{(n)}(\omega_o,\tilde\omega',Z)\right], \tag{D.6}$$

where the arguments of $\mathcal{V}^{llnn}_{jjjj}$ and $\mathcal{V}^{lnln}_{jjjj}$ are $(\omega_o, \tilde{\omega}, \tilde{\omega}', \widetilde{h}, Z)$. The expectation of $\mathcal{R}(\zeta, j)$ is computed in Proposition 6.1, and we rewrite it here as

$$|E\{\mathcal{R}(\zeta,j)\}|^2 \approx \frac{\varepsilon^{2(2-\sigma)}}{16}\left|\int_{-B}^{B}\frac{dh}{2\pi}\int_{-\Omega}^{\Omega}\frac{d\tilde{\omega}}{2\pi}\widehat{f}_B\left(h+\frac{\varepsilon^2}{2}\tilde{\omega}\right)\overline{\widehat{f}_B}\left(h-\frac{\varepsilon^2}{2}\tilde{\omega}\right)e^{-i\tilde{\omega}\zeta\beta'_j(\omega_o)}\right.$$

$$\left.\times\sum_{l=1}^{N(\omega_o)}\frac{\beta_l(\omega_o)}{\beta_j(\omega_o)}\phi_l^2(x_\star)\widehat{W}_j^{(l)}(\omega_o,\tilde{\omega},Z)\right|^2. \tag{D.7}$$

Now, let us recall from (5.29) that, as Z increases,

$$\widehat{W}_j^{(l)}(\omega_o,\tilde{\omega},Z)\to\frac{1}{N(\omega_o)}e^{i\tilde{\omega}\beta'(\omega_o)Z-\tilde{\omega}^2\sigma_e^2Z/2}. \tag{D.8}$$

It is difficult to get an explicit limit of $\mathcal{V}^{ll'nn'}_{jjjj}$ for arbitrary values of $\widetilde{h}$, $\tilde{\omega}$, and $\tilde{\omega}'$. Their maximum is attained at $\widetilde{h}=\tilde{\omega}=\tilde{\omega}'=0$, where we have from [11, section 20.9.3] that

$$\mathcal{V}^{llll}_{jjjj}(\omega_o,0,0,0,Z)\to\frac{2}{N(\omega_o)\left[N(\omega_o)+1\right]}, \tag{D.9}$$

$$\mathcal{V}^{llnn}_{jjjj}(\omega_o,0,0,0,Z)\to\frac{1}{N(\omega_o)\left[N(\omega_o)+1\right]},\quad l\neq n, \tag{D.10}$$

$$\mathcal{V}^{lnln}_{jjjj}(\omega_o,0,0,0,Z)\to\frac{1}{N(\omega_o)\left[N(\omega_o)+1\right]},\quad l\neq n. \tag{D.11}$$

Using these results and writing the probabilistic representation[4] of the transport equations obtained by taking the Fourier transform over $(\tilde{\omega}+\tilde{\omega}')/2$ and $(\tilde{\omega}-\tilde{\omega}')/2$ in Proposition D.1, for $\widetilde{h}=(\tilde{\omega}-\tilde{\omega}')/2$, we can also obtain that

$$\mathcal{V}^{ll'nn'}_{jjjj}\left(\omega_o,\tilde{\omega},\tilde{\omega}',\widetilde{h}=\frac{\tilde{\omega}-\tilde{\omega}'}{2}\right)\rightsquigarrow\mathcal{V}^{ll'nn'}_{jjjj}(\omega_o,0,0,0)e^{i(\tilde{\omega}+\tilde{\omega}')\beta'(\omega_o)Z-\left(\tilde{\omega}^2+(\tilde{\omega}')^2\right)\sigma_e^2Z/2}.$$

The choice $\widetilde{h}=(\tilde{\omega}-\tilde{\omega}')/2$ simplifies the problem in Proposition D.1 because we can set by symmetry $\mathcal{V}_{jqjq}=\mathcal{V}_{jjqq}$. The equations are much harder to analyze in the remaining cases, but we observe with direct numerical computations, which solve the system of equations in Proposition D.1, that $\mathcal{V}^{llnn}_{jjjj}$ and $\mathcal{V}^{lnln}_{jjjj}$ remain of the same order as $\widehat{W}_j^{(l)}\widehat{W}_j^{(n)}$.

Let us look closer at the sum in (D.6) and estimate it at $\widetilde{h}=\tilde{\omega}=\tilde{\omega}'=0$. We have that, as Z grows, this sum approaches

$$\frac{2}{N(N+1)}\left|\sum_{l=1}^{N}\frac{\beta_l}{\beta_j}\phi_l^2(x_\star)\right|^2-\frac{1}{N^2}\left|\sum_{l=1}^{N}\frac{\beta_l}{\beta_j}\phi_l^2(x_\star)\right|^2=\frac{N-1}{N+1}\frac{1}{N^2}\left|\sum_{l=1}^{N}\frac{\beta_l}{\beta_j}\phi_l^2(x_\star)\right|^2,$$

whereas the sum in (D.7) satisfies

$$\sum_{l=1}^{N(\omega_o)}\frac{\beta_l(\omega_o)}{\beta_j(\omega_o)}\phi_l^2(x_\star)\widehat{W}_j^{(l)}(\omega_o,\tilde{\omega}=0,Z)\to\frac{1}{N}\sum_{l=1}^{N}\frac{\beta_l}{\beta_j}\phi_l^2(x_\star).$$

[4]The probabilistic representation is obtained with a procedure similar to that in [11, section 20.6.2], but for a jump Markov process $\{J_z,Q_z\}_{z\geq0}$ with state space in $[1,\ldots,N(\omega_o)]\times[1,\ldots,N(\omega_o)]$, and with the generator given by the right-hand side of the equations in Proposition D.1.

That is, the sum in (D.6) is a factor of $(N-1)/(N+1) \approx 1$ of the sum in (D.7), in the vicinity of $\widetilde{h} = \tilde{\omega} = \tilde{\omega}' = 0$, where the terms attain their maximum. Therefore, we cannot expect a small ratio $V/|E\{\mathcal{R}\}|^2$, unless we are in a broad band regime with $\sigma < 2$.

For $\sigma < 2$, we can approximate (D.6) as

(D.12)
$$V(\zeta, j) \approx \frac{\varepsilon^{3(2-\sigma)}\Omega}{16\pi} \int_{-B}^{B} \frac{dh}{2\pi} |\widehat{f}_B(h)|^4 \sum_{l,n}^{N(\omega_o)} \frac{\beta_l(\omega_o)\beta_n(\omega_o)}{\beta_j^2} \phi_l^2(x_\star)\phi_n^2(x_\star) \int_{-\Omega}^{\Omega} \frac{d\tilde{\omega}}{2\pi} \int_{-\Omega}^{\Omega} \frac{d\tilde{\omega}'}{2\pi}$$
$$\times e^{-i(\tilde{\omega}+\tilde{\omega}')\zeta\beta_j'(\omega_o)} \left\{ \int_{-\Omega}^{\Omega} \frac{d\widetilde{h}}{2\Omega} \left[\mathcal{V}_{jjjj}^{llnn} + (1-\delta_{ln}) \mathcal{V}_{jjjj}^{lnln} \right] - \widehat{W}_j^{(l)}(\omega_o, \tilde{\omega}, Z) \widehat{W}_j^{(n)}(\omega_o, \tilde{\omega}', Z) \right\}$$

and (D.7) as

$$|E\{\mathcal{R}(\zeta, j)\}|^2 \approx \frac{\varepsilon^{2(2-\sigma)}}{16} \left[\int_{-B}^{B} \frac{dh}{2\pi} |\widehat{f}_B(h)|^2 \right]^2 \sum_{l,n}^{N(\omega_o)} \frac{\beta_l(\omega_o)\beta_n(\omega_o)}{\beta_j^2} \phi_l^2(x_\star)\phi_n^2(x_\star)$$
(D.13)
$$\times \int_{-\Omega}^{\Omega} \frac{d\tilde{\omega}}{2\pi} \int_{-\Omega}^{\Omega} \frac{d\tilde{\omega}'}{2\pi} e^{-i(\tilde{\omega}+\tilde{\omega}')\zeta\beta_j'(\omega_o)} \widehat{W}_j^{(l)}(\omega_o, \tilde{\omega}, Z) \widehat{W}_j^{(n)}(\omega_o, \tilde{\omega}', Z),$$

where

$$\left[\int_{-B}^{B} dh |\widehat{f}_B(h)|^2 \right]^2 \leq 2B \int_{-B}^{B} dh |\widehat{f}_B(h)|^4$$

by the Cauchy–Schwarz inequality. We conclude by comparing these expressions and the fact that $\mathcal{V}_{jjjj}^{llnn}$ and $\mathcal{V}_{jjjj}^{lnln}$ are of similar magnitude to $\widehat{W}_j^{(l)}\widehat{W}_j^{(n)}$, that is,

(D.14)
$$\frac{V(\zeta, j)}{\max_\zeta |E\{\mathcal{R}(\zeta, j)\}|^2} = O\left(\frac{\varepsilon^{2-\sigma}\Omega}{B} \right),$$

as stated in Proposition 6.4. ∎

REFERENCES

[1] A. B. Baggeroer, W. A. Kuperman, and P. N. Mikhalevsky, *An overview of matched field methods in ocean acoustics*, IEEE J. Oceanic Eng., 18 (1993), pp. 401–424.

[2] E. Bécache, P. Joly, and C. Tsogka, *An analysis of new mixed finite elements for the approximation of wave propagation problems*, SIAM J. Numer. Anal., 37 (2000), pp. 1053–1084.

[3] C. M. Bender and S. A. Orszag, *Advanced Mathematical Methods for Scientists and Engineers: Asymptotic Methods and Perturbation Theory*, Springer-Verlag, New York, 1999.

[4] L. Borcea, G. Papanicolaou, and C. Tsogka, *Interferometric array imaging in clutter*, Inverse Problems, 21 (2005), pp. 1419–1460.

[5] L. Borcea, G. Papanicolaou, and C. Tsogka, *Adaptive interferometric imaging in clutter and optimal illumination*, Inverse Problems, 22 (2006), pp. 1405–1436.

[6] L. Borcea, G. Papanicolaou, and C. Tsogka, *Asymptotics for the space-time Wigner transform with applications to imaging*, in Stochastic Differential Equations: Theory and Applications, Interdiscip. Math. Sci. 2, P. H. Baxendale and S. V. Lototsky, eds., World Scientific, Hackensack, NJ, 2007, pp. 91–111.

[7] L. Breiman, *Probability*, Classics Appl. Math. 7, SIAM, Philadelphia, 1992.

[8] L. Devroye, *Nonuniform Random Variate Generation*, Springer-Verlag, New York, 1986.

[9] L. B. Dozier and F. D. Tappert, *Statistics of normal mode amplitudes in a random ocean. I. Theory*, J. Acoust. Soc. Amer., 63 (1978), pp. 353–365.
[10] S. M. Flatté and F. D. Tappert, *Calculation of the effect of internal waves on oceanic sound transmission*, J. Acoust. Soc. Amer., 58 (1975), pp. 1151–1159.
[11] J. P. Fouque, J. Garnier, G. Papanicolaou, and K. Solna, *Wave Propagation and Time Reversal in Randomly Layered Media*, Springer-Verlag, New York, 2007.
[12] J. Garnier and G. Papanicolaou, *Pulse propagation and time reversal in random waveguides*, SIAM J. Appl. Math., 67 (2007), pp. 1718–1739.
[13] K. D. Heaney and W. A. Kuperman, *Very long-range source localization with a small vertical array*, J. Acoust. Soc. Amer., 104 (1998), pp. 2149–2159.
[14] W. Kohler and G. C. Papanicolaou, *Wave propagation in a randomly inhomogeneous ocean*, in Wave Propagation and Underwater Acoustics, Lecture Notes in Phys. 70, Springer-Verlag, Berlin, 1977, pp. 153–223.
[15] J. L. Krolik, *Matched-field minimum variance beamforming in a random ocean channel*, J. Acoust. Soc. Amer., 92 (1992), pp. 1408–1419.
[16] W. A. Kuperman, W. S. Hodgkiss, H. C. Song, T. Akal, C. Ferla, and D. R. Jackson, *Phase conjugation in the ocean: Experimental demonstration of an acoustic time-reversal mirror*, J. Acoust. Soc. Amer., 103 (1998), pp. 25–40.
[17] H. J. Kushner, *Approximation and Weak Convergence Methods for Random Processes, with Applications to Stochastic Systems Theory*, MIT Press, Cambridge, MA, 1984.
[18] A. Parvulescu, *Matched-signal ("MESS") processing by the ocean*, J. Acoust. Soc. Amer., 98 (1995), pp. 943–960.
[19] K. Yoo and T. C. Yang, *Broadband source localization in shallow water in the presence of internal waves*, J. Acoust. Soc. Amer., 106 (1999), pp. 3255–3269.